

**Citation for published version:**

G. P. Rosotti, et al., “Protoplanetary disc evolution affected by star–disc interactions in young stellar clusters”, *Monthly Notices of the Royal Astronomical Society*, Vol. 441(3), May 2014.

**DOI:**

<https://doi.org/10.1093/mnras/stu679>

**Document Version:**

This is the Published Version.

**Copyright and Reuse:**

© 2014 The Authors Published by Oxford University Press on behalf of the Royal Astronomical Society.

Content in the UH Research Archive is made available for personal research, educational, or non-commercial purposes only. Unless otherwise stated all content is protected by copyright, and in the absence of an open licence permissions for further reuse of content should be sought from the publisher, author or other copyright holder.

**Enquiries**

If you believe this document infringes copyright, please contact the Research & Scholarly Communications Team at [rsc@herts.ac.uk](mailto:rsc@herts.ac.uk)

# Protoplanetary disc evolution affected by star–disc interactions in young stellar clusters

Giovanni P. Rosotti,<sup>1,2,3★</sup> James E. Dale,<sup>2,3</sup> Maria de Juan Ovelar,<sup>4</sup>  
David A. Hubber,<sup>2,3</sup> J. M. Diederik Kruijssen,<sup>5</sup> Barbara Ercolano<sup>2,3</sup>  
and Stefanie Walch<sup>5</sup>

<sup>1</sup>Max-Planck-Institut für extraterrestrische Physik, Giessenbachstraße, D-85748 Garching, Germany

<sup>2</sup>Excellence Cluster Universe, Boltzmannstr. 2, D-85748 Garching, Germany

<sup>3</sup>Universitäts-Sternwarte München, Scheinerstraße 1, D-81679 München, Germany

<sup>4</sup>Leiden Observatory, Leiden University, PO Box 9513, NL-2300 RA Leiden, the Netherlands

<sup>5</sup>Max-Planck-Institut für Astrophysik, Karl-Schwarzschild-Str. 1, D-85748 Garching, Germany

Accepted 2014 April 4. Received 2014 April 4; in original form 2013 October 11

## ABSTRACT

Most stars form in a clustered environment. Therefore, it is important to assess how this environment influences the evolution of protoplanetary discs around young stars. In turn, this affects their ability to produce planets and ultimately life. We present here for the first time 3D smoothed particle hydrodynamics/ $N$ -body simulations that include both the hydrodynamical evolution of the discs around their natal stars, as well as the dynamics of the stars themselves. The discs are viscously evolving, accreting mass on to the central star and spreading. We find penetrating encounters to be very destructive for the discs as in previous studies, although the frequency of such encounters is low. We also find, however, that encounter influence the disc radii more strongly than other disc properties such as the disc mass. The disc sizes are set by the competition between viscous spreading and the disruptive effect of encounters. As discs spread, encounters become more and more important. In the regime of rapid spreading, encounters simply truncate the discs, stripping the outer portions. In the opposite regime, we find that the effect of many distant encounters is able to limit the disc size. Finally, we predict from our simulations that disc sizes are limited by encounters at stellar densities exceeding  $\sim 2\text{--}3 \times 10^3 \text{ pc}^{-2}$ .

**Key words:** accretion, accretion discs – hydrodynamics – protoplanetary discs.

## 1 INTRODUCTION

Stars form in regions of enhanced ambient gas and stellar densities compared to the Galactic field (Lada & Lada 2003). Whether or not these density peaks are long-lived or disperse on a dynamical time (i.e. whether they become bound stellar clusters or unbound associations) depends crucially on their initial densities and the resulting star formation efficiencies (Kruijssen et al. 2012). In Milky Way-like galaxies, about 10 per cent of all stars are born in bound stellar clusters (Bastian 2008), but this number increases with the gas surface density to up to  $\sim 50$  per cent in high-density starburst environments (Goddard, Bastian & Kennicutt 2010; Adamo, Östlin & Zackrisson 2011; Kruijssen 2012; Silva-Villa, Adamo & Bastian 2013).

The cluster environment leaves a spectacular imprint on the star formation process. Through the collective feedback of young stars such as stellar winds and photoionizing radiation, natal gas is ejected

and the accretion discs surrounding protostars may be destroyed by external photoevaporation (Adams et al. 2004; Pelupessy & Portegies Zwart 2012; Dale, Ercolano & Bonnell 2013). Combining the current observational and theoretical understanding of planet-, star-, cluster- and galaxy formation, Longmore et al. (2014) estimate that some 10 per cent of all stars in the Universe may have the formation of planets (or lack thereof) in their habitable zones affected by their natal cluster environment. In this paper, we concentrate on the dispersal of gas from protoplanetary discs through encounters with neighbouring stars. It serves as a first step to obtaining a detailed understanding of how the cluster environment affects the evolution of protoplanetary discs.

In isolation, an effective viscosity causes the redistribution of angular momentum within the gaseous disc (Lynden-Bell & Pringle 1974). This leads to disc spreading on the one hand and mass accretion on to the central star on the other hand. While the latter process is routinely observed (e.g. Gullbring et al. 1998; Natta et al. 2004; Herczeg & Hillenbrand 2008; Manara et al. 2012), there are only a few observational reports of disc spreading (Isella, Carpenter & Sargent 2009; Guilloteau et al. 2011), as high spatial resolution is

\* E-mail: [rosotti@usm.lmu.de](mailto:rosotti@usm.lmu.de)

needed to resolve the disc size. Within the current limitations, these works show how simple theoretical models are able to reproduce the observed rate of disc spreading. In practice, these works have concentrated on the nearest star-forming regions (SFR), namely Taurus-Auriga and Ophiucus, which are characterized by a lower stellar density when compared with more crowded regions, like the Orion nebula Cluster (ONC). After several Myr of this slow and quiet evolution, it appears that another destructive process kicks in, and the disc is rapidly cleared on an  $\sim 10^5$  yr time-scale (Luhman et al. 2010; Ercolano, Clarke & Hall 2011; Koepferl et al. 2013). Currently, internal photoevaporation is the best candidate mechanism for such a fast disc dispersal (Clarke, Gendrin & Sotomayor 2001; Alexander, Clarke & Pringle 2006; Gorti, Dullemond & Hollenbach 2009; Owen et al. 2010; Owen, Ercolano & Clarke 2011).

Does a clustered environment impact this picture of disc evolution? de Juan Ovelar et al. (2012) found evidence of a dependence of the observed disc sizes on the environmental surface stellar density. In particular, discs in crowded environments, that is, at stellar densities above  $10^{3.5} \text{ pc}^{-2}$ , are systematically smaller than their counterparts in less crowded fields. Observationally, it is known that proximity to high-mass stars may alter the evolution of protoplanetary discs via external photoevaporation (O'dell 1998; Mann & Williams 2010; Miotello et al. 2012). The high-energy radiation from massive stars can ionize and evaporate the material in the atmosphere of discs even at distances of  $\simeq 1$  pc (Johnstone, Hollenbach & Bally 1998; Adams et al. 2004). Although there are spectacular images of this process in silhouette discs (proplyds) in the ONC, overall this process is not expected to be the main driver of disc evolution (Adams 2010). Another important process occurring in a clustered environment are stellar encounters. Most of the previous works done on this problem has concentrated on modelling a given existing stellar cluster. These studies (Sclally & Clarke 2001; Olczak, Pflanzner & Spurzem 2006; Pflanzner, Tackenberg & Steinhausen 2008; Olczak et al. 2012; Craig & Krumholz 2013) involved either semi-analytic solutions or pure  $N$ -body simulations in which close stellar encounters are recorded and the effect of single encounters on a putative disc is inferred a posteriori (using results from simulations with pure  $N$ -body techniques, or including also hydrodynamical effects).

Sclally & Clarke (2001) performed  $N$ -body simulations using 4000 stars in virial equilibrium in an  $r^{-2}$  density distribution with a half-mass radius of  $\sim 1$  pc to model the ONC. The ONC is a popular target, being the nearest massive SFR, where many protostellar discs are observed in silhouette against the bright nebula (Ricci, Robberto & Soderblom 2008; Robberto et al. 2013). The ONC contains  $\sim 4000$  stars (i.e.  $\sim 2 \times 10^3 M_{\odot}$ ) in an  $\sim 5$  pc diameter volume, has a one-dimensional velocity dispersion of  $2.5 \text{ km s}^{-1}$  and a core density of  $4.7 \times 10^4 \text{ pc}^{-3}$ . Sclally & Clarke (2001) found that  $\sim 8$  per cent of all stars and  $\sim 30$  per cent of core stars suffered a sub-100 au encounter after 12.5 Myr of integration and concluded that encounters were unlikely to significantly affect the disc population. However, they cautioned that the sharp outer cut-off in their stellar distribution caused their models to expand significantly. This naturally lowers the encounter rate.

Olczak et al. (2006) used very similar initial conditions to Sclally & Clarke (2001) in their  $N$ -body study of the ONC, except that they also modelled sub-virial clusters. Instead of recording the single closest encounter, as in Sclally & Clarke (2001), Olczak et al. (2006) recorded the complete encounter history of objects on the following grounds: (a) the closest encounter may not be the most destructive, since a distant flyby of a massive perturber can do more

damage than a near-miss with a low-mass object (Moeckel & Bally (2007) found that unequal-mass encounters are more destructive); (b) some stars will experience several encounters whose effects may be cumulative. They also concluded that the fraction of stars experiencing sub-100 au encounters in 12.5 Myr was small, at most  $\sim 12$  per cent. They estimated disc mass-losses explicitly using a fitting formula from an extension of the parameter-space study of Pflanzner et al. (2005a) and found that serial encounters and flybys of massive perturbers were able to affect the disc population, at least in the dense core of the cluster. They concluded that, over 12.5 Myr,  $\sim 4$  per cent of discs in the ONC and  $\sim 10$  per cent of discs in the core would be destroyed outright, assuming initial disc radii of 100 au. This fraction is increased to  $\sim 9$  and  $\sim 20$  per cent, respectively, if initial outer disc radii of 200 au are assumed instead.

Pflanzner et al. (2008), again considering the ONC, pointed out that close encounters involving disc-bearing stars in clusters can also result in bursts of accretion due to spiral arms induced in the discs. They concluded that this is a common phenomenon in dense cluster cores, driving accretion rates up by orders of magnitude for short periods ( $10^2$ – $10^4$  yr), during which 5–10 per cent of the disc may be accreted. Pflanzner (2008) speculated that such events may be observed as FU Orionis outbursts.

Olczak et al. (2012) studied star–disc interactions in the Arches cluster. The Arches is more massive ( $\sim 3 \times 10^4 M_{\odot}$ ), more compact (with a half-mass radius of  $\sim 0.4$  pc) and therefore much denser ( $\sim 2 \times 10^5 \text{ pc}^{-3}$ ) than the ONC. It also has a higher one-dimensional velocity dispersion ( $5.4 \text{ km s}^{-1}$ ). Encounter rates are therefore expected to be substantially higher in this system and, since its age is comparable to that of the ONC (a few Myr), the total number of encounters that have already occurred should also be much higher. Observations by Stolte et al. (2010) revealed that the disc fraction in the Arches cluster is an increasing function of distance from the cluster centre, rising from a few per cent in the core to around 10 per cent at a radius of 0.3 pc. Olczak et al. (2012) again employed  $N$ -body modelling, and post-processing with techniques similar to Olczak et al. (2006) to infer disc mass-losses. They found disc destruction fractions of 10 per cent in the entire cluster and 30 per cent in the core over 2.5 Myr.

Malmberg et al. (2007) and Malmberg, Davies & Hoggie (2011) performed  $N$ -body simulations of clusters containing a number of stars ranging from 150 to 1000 and half-mass radii ranging from 0.38 to 7.66 pc. They quantified from the simulations the fraction of singletons, which they define as those stars that never had encounters closer than 1000 au. They found that in some cases almost  $\sim 85$  per cent of stars are non-singletons, with potential impact on planet-forming protoplanetary discs and already existing planetary systems. They also found frequent exchange of stars in binaries. The effect of flybys on already formed planetary systems is to lead to planet ejection and eccentricity excitation in planets that are left in the system, as well as increasing the probability of planet–planet scattering after the flyby. These authors note that due to binary heating, which will lead to a significant cluster expansion, most encounters happen when the cluster is very young, and therefore the impact on protoplanetary discs can be significant.

Craig & Krumholz (2013) performed  $N$ -body simulations of a set of idealized, fractally substructured clusters. Since the local stellar density in cluster sub-groups can greatly exceed the average density, the encounter rates in a structured cluster should be considerably higher than in a smooth cluster with otherwise comparable properties. However, stellar sub-groups are dynamically erased on a crossing time in bound systems, so it is not obvious that the total

number of encounters will be higher in a structured cluster. Craig & Krumholz (2013) found that the overall enhancement in the number of encounters due to sub-structure is only a factor of a few, and that discs in such clusters are not likely to be significantly dynamically influenced in this way.

In this paper, we present results from hybrid  $N$ -body–smoothed particle hydrodynamics (SPH) simulations of coupled cluster and protoplanetary disc evolution. Therefore, we do not need to infer a posteriori the effect of encounters on discs, but we compute it self-consistently together with the stellar dynamics. This allows us to include effects that were neglected in previous studies:

- (i) disc spreading and truncation by encounters;
- (ii) accretion on to the central star;
- (iii) the finite time for a disc to regain equilibrium after an encounter;
- (iv) the inclination of the rotation axis with respect to the inclination of the two stars' orbital plane, which has an important effect (it is well known, for example, that a retrograde passage is much less harmful for the disc than a prograde one);
- (v) disc–disc interactions, if both stars in an encounter have a disc;
- (vi) the mass transfer between stars, possibly leading to the formation of a new disc.

Rather than trying to accurately reproduce one particular stellar cluster, we concentrate here on an idealized model. This allows us to work in a controlled environment, identifying the new phenomena that arise due to the new computational method adopted. At this stage, we are able to make some preliminary comparison with observations. The questions we want to answer are as follows.

- (i) How important are stellar encounters for disc dispersal?
- (ii) What are the conditions under which disc sizes are set by stellar encounters?
- (iii) Are there observables in protoplanetary discs that can tell us if a disc or a disc population experienced significant encounters?

Our paper is organized as follows. After describing the computational method in Section 2, we present our results in Section 3. We discuss them in Section 4, comparing with results from a simple semi-analytical method and with observations, and we draw our conclusions in Section 5.

## 2 MODEL

### 2.1 Numerical method

We use the SPH code *SEREN* (Hubber et al. 2011). *SEREN* is capable of modelling both the hydrodynamics and stellar dynamics individually, or coupled together in the same simulation (Hubber et al. 2013a). The equations of motion are derived via the Euler–Lagrange equations, similar to the derivations of Springel & Hernquist (2002) and Price & Monaghan (2007), but including the coupled gas–star terms to maintain energy conservation. The SPH particles are integrated using a second-order Leapfrog kick-drift-kick integration scheme and the star particles are integrated with a fourth-order Hermite integration scheme. The equations of motion for both the SPH and star particles are integrated on hierarchical block timesteps. The smoothing lengths of SPH particles are calculated with the following relation:

$$h_i = \eta \left( \frac{m_i}{\rho_i} \right)^{1/3}, \quad (1)$$

where  $\eta = 1.2$  and  $\rho_i$  is the SPH density. We use the M4 kernel (Monaghan & Lattanzio 1985) for calculating all SPH sums.

We employ an ideal gas equation of state, assuming a mean molecular weight  $\mu = 2.35$ . Due to the already high computational demands of running a cluster simulation with gas dynamics, we use a simplified approach to modelling the thermal and radiation physics: the temperature of each SPH particle depends only on its position relative to the central star (we explain in detail in Section 2.2.2 how particles temperatures are assigned). Therefore, we do not need to solve the energy equation, nor alternative forms such as the entropy equation.

In order to capture shocks and prevent interpenetration of particles, SPH needs to include an artificial viscosity term. We use the term proposed by Monaghan (1997) of the form,

$$\left. \frac{d\mathbf{v}_i}{dt} \right|_{AV} = \sum_{j=1}^N \frac{m_j \alpha_{AV} v_{SIG} \mathbf{v}_{ij} \cdot \hat{\mathbf{r}}_{ij}}{\bar{\rho}_{ij}} \nabla_i W_{ij}, \quad (2)$$

where  $\alpha_{AV}$  is a dimensionless factor of order unity and  $v_{SIG} = c_i + c_j - \beta_{AV} \mathbf{v}_{ij} \cdot \hat{\mathbf{r}}_{ij}$  is the signal speed between neighbouring SPH particles, with  $\beta_{AV} = 2\alpha_{AV}$ . In order to capture shocks,  $\alpha_{AV} = 1$  usually suffices for adiabatic shocks for all Mach numbers (e.g. Hubber, Falle & Goodwin 2013b). It can be shown (Artymowicz & Lubow 1994; Murray 1996) that the artificial viscosity term can also be used to model the physical viscosity that is responsible in accretion discs for the redistribution of angular momentum. An unwanted effect is that in this case the artificial viscosity results in both bulk viscosity, which is required to capture shocks, and shear viscosity, which is the only one required in accretion discs. In practice, this is usually not a major problem in simulations of accretion discs, as bulk viscosity acts on strongly convergent flows, which are usually not present in accretion discs.

The effective shear viscosity is resolution dependent, and since our simulations have a relatively low resolution on the scale of individual discs, the effective shear viscosity is very high, leading to rapid viscous evolution of discs. Although a variety of viscosity switches exist in SPH that attempt to address this problem (e.g. Balsara 1995, Morris & Monaghan 1997), we simply adopt a lower value of  $\alpha_{AV} = 0.1$  in all our simulations. Although this has the unwanted side effect of reducing the ability to capture strong shocks, this is a smaller problem than the high shear viscosity for our simulations. In the next section, we discuss the link between our numerical parameters and the physical values of the viscosity expected in protoplanetary discs.

To model the accretion of gas on to stars, we use sink particles similar to those described by Bate, Bonnell & Price (1995) and Hubber et al. (2011). The smoothing length of sink particles is simply  $R_{in}/2$  for close encounters between sinks, where  $R_{in}$  is the sink accretion radius, whose value will be given in the next section. We do not allow the formation of new sinks, only the accretion of SPH particles on to existing sink/star particles. Indeed, we do not expect new sinks to form both for numerical and physical reasons. Physically, the masses contained in the discs are too low to form new stars and the discs are not gravitationally unstable. In addition, other works (Lodato et al. 2007; Forgan & Rice 2009) have shown that encounters between stars prohibit the fragmentation of discs and stabilize them. Also, the numerical resolution is too low to follow the formation of planet-sized objects by gravitational instability (Bate & Burkert 1997).

## 2.2 Physical set-up

### 2.2.1 Cluster set-up

Our model comprises two particle species, stars and gas. We choose to perform a controlled experiment and model the cluster dynamics as simply as possible by employing a Plummer sphere of 100 equal-mass stars. The Plummer sphere has a density profile given by

$$\rho(r) = \frac{3M}{4\pi a^3} \left(1 + \frac{r^2}{a^2}\right)^{-5/2}, \quad (3)$$

where  $M$  is the cluster mass and  $a$  is a scale-radius, normally called the Plummer radius. The procedure used to generate the sphere is described in Aarseth, Henon & Wielen (1974), which describes also how to initialize the velocities under the assumption that the velocity distribution is isotropic. Because of their simplicity, Plummer spheres have been commonly used in previous works when dealing for the first time with a new numerical technique (Lada, Margulis & Dearborn 1984; Pelupessy & Portegies Zwart 2012). Since the Plummer sphere density profile theoretically extends to infinity, we truncate it at 20 times the Plummer radius. We use dimensionless units in which the radius and the mass of the Plummer sphere is 1, so that our results can be rescaled to different cluster sizes and masses. However, we note that for each given simulation the ratio between the star and disc mass, and correspondingly between the cluster and the disc size, stays constant when rescaling. In the rest of the paper, we assume that each star has a mass of  $1 M_{\odot}$  and that the Plummer radius is 0.1 pc. We then scale all other quantities accordingly.

In the spirit of performing a controlled experiment, binaries are not included. As discussed by Olczak et al. (2012), this underestimates the effect of encounters by reducing the number of stars. In addition, binaries might have also an effect on the long term evolution of the cluster, since the binding energy of a single binary can easily be larger than the binding energy of the whole cluster. On the relaxation time-scale, binary heating leads to expansion of the cluster, which would instead cause a decrease in the importance of encounters. As we discuss in Section 3, the relaxation time-scale is, however, longer than the time span we simulate. In addition, this level of sophistication would require a better dynamical model of the cluster than the Plummer sphere we employ here.

### 2.2.2 Disc set-up

The only gas initially present is in the discs; we do not include any diffuse gas. Observations of SFR show that, even in very young regions, a fraction of young stars show no sign of infrared excess or accretion (Fedele et al. 2010). It could be that the discs of these stars have undergone a different, more rapid evolutionary path than the one of the discs we still observe. Recent work suggests that stars that do no longer have a disc are binary stars (Kraus et al. 2012). Another possibility is that the age spread between stars must account for this difference (although this is probably small, see Longmore et al. 2014). Therefore, we add a randomly oriented gas disc around 50 per cent of the stars.

The surface density profile of the gas is given by a power-law, with a slope of  $p = 3/2$  as estimated for the Minimum Mass Solar Nebula (Hayashi 1981):

$$\Sigma(R) = \Sigma_0 \left(\frac{R}{R_0}\right)^{-p}, \quad (4)$$

where  $R$  is the distance from the star in the disc plane,  $R_0$  is a scale radius and  $\Sigma_0$  is a surface density scale. The particles are distributed so as to attain a Gaussian density profile in the vertical direction, with thickness  $H = c_s/\Omega$ , where  $c_s$  is the gas sound speed and  $\Omega$  the Keplerian orbital frequency around the star. We choose  $\Sigma_0$  as to set the initial disc mass to be 5 per cent of the stellar mass. The disc is truncated at the initial disc radius  $R_{\text{out}}$ , and the inner disc radius is set to  $R_{\text{in}} = R_{\text{out}}/5$ . The true  $R_{\text{in}}$  is of the order of the star radius, but it is not possible to resolve it, because of the very short orbital time-scale there. Note that, as the disc expands,  $R_{\text{in}}$  stays constant, and the difference in the particle orbital time-scales increases. If particles move to within  $R_{\text{in}}$  of the star, they are accreted and removed from the simulation.

The temperature structure in the disc follows a power-law distribution with radius:

$$T(R) = T_0(R/R_0)^{-q}. \quad (5)$$

We choose the exponent  $q$  to be 1.5 for numerical convenience, although observations (e.g. Andrews & Williams 2005) find flatter distributions, with a median value of 0.58. Our approach has the numerical advantage that it gives a constant vertical resolution and a constant  $\alpha_{\text{SS}}$  parameter in the disc (Lodato & Pringle 2007; Lodato & Price 2010), where  $\alpha_{\text{SS}}$  is the standard viscosity parameter proposed by Shakura & Sunyaev (1973). The  $\alpha_{\text{SS}}$  parameter is related to the kinematical viscosity  $\nu$  of the gas by the prescription  $\nu = \alpha_{\text{SS}} c_s H$ . We fix the normalization  $T_0$  in equation (5) so that the aspect ratio of the disc  $H/R$  is 0.05 at the inner radius. At each timestep, we use the distance from the nearest star to set the temperature of each SPH particle. For simplicity, we use the spherical distance rather than the distance in the disc plane, as this would require to identify at each timestep the discs and find their axis, adding extra computational cost to the simulation. In practice, the difference introduced is marginal for particles in a thin disc, and it affects only particles that get ejected by the discs. For these particles, using the distance in the disc plane would be questionable anyway. Finally, to prevent unphysically low temperatures, we impose a lower threshold corresponding to the one at a distance of  $7R_{\text{in}}$ , which for run R10 corresponds to 20 K.

We run simulations with  $R_{\text{out}} = 10, 30, 100$  and  $300$  au, which will be referred to in the text as R10, R30, R100 and R300, respectively. The parameter  $R_{\text{out}}$  can be interpreted not only as the initial disc size at the beginning of the class II phase, but also as the age of the disc at the beginning of the simulation, where bigger discs are ‘old’ discs (due to viscous spreading) and the different simulations represent different evolutionary stages. Clearly, this is not fully self-consistent as we are ignoring the effect of the encounters in the expansion that brought the discs to reach these sizes. Nevertheless, since observations (Williams & Cieza 2011) show that protoplanetary discs can reach these sizes, it is interesting to know what is the effect of encounters on such discs.

We initially populate the discs with SPH particles by Monte Carlo sampling the surface density distribution given in equation (4). This causes small random fluctuations which are erased on an orbital time-scale and do not affect our results. The particles are initialized in Keplerian orbit around their stars. Our resolution is  $10^4$  particles per disc, resulting in a total number of  $5 \times 10^5$  particles for each simulation. At this resolution, using the relations in Lodato & Pringle (2007) shows that the discs are barely vertically resolved, that is,  $h/H \simeq 1$ , where  $h$  is the SPH smoothing length. We also check in the simulation output files that this is the actual resolution in the vertical direction. We compute the scaleheight of the disc through the standard deviation of the vertical coordinate of

the particles comprising the disc and by fitting a Gaussian profile to the density. We find that the two methods give the same answer within a factor of  $\sim 1.5$ . In all cases, the ratio  $h/H$  is between 1 and 2.

Our choice of the resolution allows the possibility of simulating a long timespan (for run R10, we simulate 170 000 orbits at the inner radius) and many discs at the same time, rather than being able to follow the detailed behaviour of the individual discs. A similar resolution has been employed in studies of star–star encounters (Heller 1995; Pfalzner, Umbreit & Henning 2005b). In particular, Pfalzner et al. (2005b) reported no significant difference between a simulation run with  $10^4$  particles and one with  $10^6$  particles. However, due to the accretion of particles on to the star, our spatial resolution degrades as the simulation progresses. For example, at the end of simulation R10, only  $\sim 10$  per cent of the particles are left in the discs; when combined with the disc spreading, the analytical relations predict a degradation in the spatial resolution of a factor of 3. The actual values extracted from the simulation are however still in the same range as at the beginning of the simulation. We warn however that this does not mean that the actual resolution is higher than what we would expect; rather, it means that by definition it is not possible to resolve in the simulation features that are smaller, within a factor of order unity, than  $h$ . The interpretation of this result is thus that at the end of our simulations the discs are, for numerical reasons, thicker than what is expected from their temperatures.

It is possible to compute the resulting viscosity from the chosen density and temperature profiles. According to Lodato & Price (2010), in our simulations the Shakura–Sunyaev parameter is  $\alpha_{SS} \simeq 0.004$ , which is in line with the observational results (Armitage 2011). A possible concern is that the analytical relations do not hold at the resolutions employed in this paper. For this reason, in the next section we measure explicitly the value of the viscosity by measuring the rate of spreading of the disc. Indeed, we find the effective viscosity is higher than predicted by this estimate, yet still marginally compatible with the values found in observations.

### 2.3 A semi-analytical model for the disc size

In this section, we present a semi-analytical model that we will use in Section 4.1 to understand the results of the simulation in terms of disc sizes. A class of widely used models for a disc in isolation are the family of self-similar solutions derived by Lynden-Bell & Pringle (1974). They describe the evolution of a disc whose viscosity profile is a power law. The radius–time evolution is given by

$$R_{\text{disc}}(t, R_0, t_{v,0}) = \left(1 + \frac{t}{t_{v,0}}\right)^{1/(2-\gamma)} R_0, \quad (6)$$

where  $R_0$  is the initial radius,  $t_{v,0}$  the viscous time at the initial radius and  $\gamma$  is the exponent of the viscosity with respect to radius. The viscous time can be related to the  $\alpha_{SS}$  (see Section 2.2.2) parameter using the definition of viscous time (see equation 20 of Hartmann et al. 1998) and standard relations:

$$\alpha_{SS} = \frac{1}{6\pi} \left(\frac{t_{v,0}}{t_{\text{dyn}}}\right)^{-1} (H/R)^{-2} \frac{1}{(2-\gamma)^2}, \quad (7)$$

where  $t_{\text{dyn}}$  is the orbital time-scale at  $R_0$  and  $H/R$  is the aspect ratio. For simplicity, we will use  $H/R = 0.05$  when evaluating this relation numerically. We note that this is a worst-case scenario (that is, a slightly overestimate of  $\alpha_{SS}$ ), as this is the value at the inner radius and the aspect ratio is a mildly growing function of radius. In addition, if the disc is vertically underresolved, the effective  $H$  will

be thicker than the one due to thermal pressure, therefore leading to a higher  $H/R$  and therefore to a lower  $\alpha_{SS}$  than the estimate we get.

The expansion law has the nice feature that, being self-similar, one is always free to ‘reset’ what we call initial radius, and start the evolution again from there, without changing the results (provided we also update the viscous time). In mathematical terms,

$$R_{\text{disc}}(t'', R_0, t_{v,0}) = R_{\text{disc}}(t'' - t', R_1, t_{v,1}), \quad (8)$$

where  $R_1 = R_{\text{disc}}(t', R_0, t_{v,0})$  and  $t_{v,1}$  is the viscous time at  $R_1$ .

We exploit this property in our simple semi-analytical model. We let the disc increase in size at each timestep following equation (6). In order to derive the parameters, we use numerical fits to the results of the evolution of discs in isolation. At each timestep, we look in the results of the simulation for the closest star at that time to a given disc and record its distance  $d$ . We assume that the encounter would have truncated the disc at  $d/3$  (Adams 2010). If the radius is larger than this value, we truncate the disc, otherwise we leave the disc unperturbed. We then let the viscous evolution start again. To summarize, we can compute the final disc radius assuming that:

- (i) the radius evolution is always given by equation (6), i.e. by the Lynden-Bell & Pringle (1974) solution;
- (ii) the encounter distances come from the results of the simulations;
- (iii) the encounters simply truncate the discs at  $d/3$ .

We do not expect such a simple model to be able to capture the full results of the 3D hydro simulation; however, it is useful to assess if the encounters produce a simple truncation or have more complicated effects. As we will show, the fact that there are cases where the model is capable of correctly reproducing some of the results shows that it is a useful tool. In particular, it highlights that in these cases the assumptions that have been used to build it are valid. On the contrary, when the model breaks down it shows that these assumption must have broken down.

## 3 SIMULATIONS

We evolve the clusters for 10 dynamical time-scales, where the dynamical time is defined as

$$t_{\text{dyn}} = \left(\frac{r_{\text{cluster}}^3}{GM_{\text{cluster}}}\right)^{1/2}. \quad (9)$$

Here,  $G$  is the universal gravitational constant,  $M_{\text{cluster}}$  is the total mass of the cluster and  $r_{\text{cluster}}$  is the scalelength  $a$  of the Plummer sphere (see equation 3). For the scalelength (0.1 pc) and mass values ( $100 M_{\odot}$ ) introduced in Section 2.2, the dynamical time-scale is  $\simeq 47\,000$  yr. Therefore, the simulations are evolved for  $t_{\text{end}} = 0.47$  Myr. For example, after this time in simulation R10, nearly 90 per cent of the initial mass has accreted on to the stars.

Our cluster will evolve on the relaxation time, which is given by

$$t_{\text{relax}} = \frac{N}{\ln(0.4N)} t_{\text{dyn}} \simeq 27 t_{\text{dyn}} \simeq 1.27 \text{ Myr}. \quad (10)$$

Given that this time is longer than the one we simulate, we do not expect a significant evolution of the cluster during the simulation due to pure  $N$ -body effects. The relaxation time is of the same order as the lifetime of protoplanetary discs (3 Myr; Fedele et al. 2010). This means that during the life of a protoplanetary disc there will be some evolution of the cluster. This is important when interpreting discs with large outer radii as discs which have already evolved due to viscous spreading. In this case, the simulation is not fully

self-consistent since we do not simulate the early dynamical evolution of the cluster but start from the same cluster initial conditions.

### 3.1 Extracting the discs from the simulation

To analyse the results of the simulations, we apply a procedure to extract the discs. Each gas particle is assigned to the star that it is most bound to. We also apply a cut-off in eccentricity of 0.9, but in practice we find that very few bound particles have such high eccentricities. We define the *ambient gas* as particles that are not bound to any star. Once we have identified a disc, in order to find its plane we apply the algorithm already used in Walch et al. (2010). We compute the inertia tensor of the disc, defined as (Landau & Lifshitz 2010)

$$I_{ij} = \sum_a m_a (x_a^2 \delta_{ij} - x_{i,a} x_{j,a}), \quad (11)$$

where  $x_a$  is the position vector of each particle in the disc with respect to the star,  $\delta_{ik}$  the Kronecker delta,  $m_a$  the mass of each particle and the summation over index  $a$  is running over all the particles in the disc, while the indices  $i, j = \{x, y, z\}$  are for coordinate axes. It can be shown that, in the limit of a razor thin axisymmetric disc, the eigenvalues of the tensor  $I_{x'}$ ,  $I_{y'}$ ,  $I_{z'}$  are such that  $I_{x'} = I_{y'} + I_{z'}$ , where  $I_{z'}$  is the eigenvalue corresponding to the eigenvector along the rotation axis  $z'$  of the disc, while the other two eigenvectors lie in the plane of the disc. Therefore, to identify the plane, we diagonalize the tensor and define the direction of the eigenvector with the largest eigenvalue as the direction of the disc axis. Since the disc is a continuous structure without an abrupt end, we compute the radius of the disc as the half-mass Lagrangian radius, that is, the radius that contains half the mass of the disc. If the evolution of the disc remains purely viscous, the surface density follows one of the self-similar solutions found by Lynden-Bell & Pringle (1974) and the Lagrangian radius is proportional to the exponential tapering radius of the self-similar solution (e.g. Hartmann et al. 1998). The self-similar solution is used in sub-millimetre observations to fit the surface density profile and derive the disc size (Williams & Cieza 2011); therefore, it is important that our method is able to give consistent results in this case.

### 3.2 Spreading in isolation

In order to compare the model presented in Section 2.3 with the results of the simulation, we need to know the disc expansion law. In principle, if we were to know exactly our viscosity law, we could use it to derive our expansion law. In practice, since we cannot afford a very high resolution due to computational limitations, we have to instead rely on calibrations, that are derived by fitting the evolution of a disc in isolation.

We show in Table 1 the parameters of the fit, together with the corresponding value of the effective viscosity  $\alpha_{SS}$  computed using equation (7). We note that these values are higher than those pre-

dicted from the analytical relations (by a factor of 40 in the worst case). Typical values for  $\alpha_{SS}$  range from  $10^{-2}$  to  $10^{-4}$ , so that our discs are quite viscous. From the analytical relations, we would expect a constant  $\alpha_{SS}$ , and therefore a constant viscosity, which should translate to  $\gamma = 0$ . Since we get a different value, this means at these resolutions the analytical formulae for SPH viscosity are not valid. On the other hand, this is an effect that we can calibrate for. Although we cannot decide which viscosity law to apply, we can still derive it a posteriori by looking at the evolution of a disc in isolation. This also means however that care should be taken when interpreting the value of  $\alpha_{SS}$  reported in the table. This value is to be interpreted as a *global*, effective value that describes how fast overall the disc is expanding. However, the *local*, that is, at  $R_{out}$ , level of angular momentum transport is higher than this. This is important as it is this local level that determines the ability of the disc to wash out local perturbations. For reference, we report in the table also the *local* values of  $\alpha_{SS}$ , that we compute from the formula (e.g. Armitage 2011):

$$\alpha_{SS,local} = \frac{1}{2\pi} \left( \frac{t_{v,0}}{t_{dyn}} \right)^{-1} (H/R)^{-2}. \quad (12)$$

We note that the different runs have quite different expansion laws. In particular, it is the exponent in the relation that tends to vary the most. Some of the discs show values of  $\gamma$  that are clearly unphysical: for example, the value  $-3$  for R300 implies a very steep and increasing dependence of the temperature with radius, which is not present in our model. Therefore, one should regard the Lynden-Bell & Pringle (1974) similarity solution as a fitting formula for the evolution of these discs, and not as a *physical* description of their evolution. For this reason, the local estimate of  $\alpha_{SS}$  is a more accurate description of what is going on in these simulations. Viscosity values are expected to be lower in real discs, which implies that those encounters' effects that in our simulations could not be washed out by viscosity would be even stronger in real discs. The variation of the exponent means that, despite the fact that the viscous times are similar, run R10 is the one varying the fastest (indeed, it even overtakes the other ones by the end of the simulation), while the other ones expand more slowly. For this reason, we stress that looking only at the viscous time might be misleading, since this value alone does not fully describe the evolution of the disc. As another reference, we list in the table also the value of  $t_{spread}$ , which we define as

$$t_{spread} = \frac{R_{disc}}{dR/dt}, \quad (13)$$

that is, the time-scale for a significant change in the disc radius. We evaluate the denominator by computing analytically the derivative of equation 6, and use the value of  $R_{disc}$  at  $t = 0$ . It can be seen that the disc R10 is the one that is varying the fastest. It is reassuring that the disc in run R300, the one with the highest value of  $\alpha_{SS}$ , has a very long  $t_{spread}$ , so that its spreading is quite limited during the course of the simulation (see also Fig. 7).

In order to quantify the effect of the limited resolution available on the viscosity, we run resolution tests of the discs in isolation, that we report in the appendix.

The viscosity is also important after an encounter, as it allows for the particle orbits to circularize. As Clarke & Pringle (1993) pointed out, the exact form of the viscosity law probably does not matter (in fact, some of the simulations in the literature have been done only with pseudo-viscosity) for what the final surface density distribution after an encounter is. Indeed, the final surface density is given by the particle specific angular momentum, which sets the

**Table 1.** For each simulation run, we show the parameters of the fit to the radius–time relation with the analytical solution given by equation (6).

Run	$R_{out}$ (au)	$\gamma$	$t_v$ (yr)	$\alpha_{SS}$	$t_{spread}$ (yr)	$\alpha_{SS,local}$
R10	10	1.11	18 891	0.045	16 800	0.1
R30	30	0.44	23 218	0.062	36 220	0.45
R100	100	−1.69	11 762	0.133	43 400	5.4
R300	300	−3.19	25 432	0.161	132 000	13

final distance from the star once all the orbits have circularized. This is true if there are no further encounters, but the exact viscosity that one assumes decides the time-scale over which the disc finds a new equilibrium after an encounter. This is important in our simulation, as the outcome of a second encounter will be different depending on whether the disc had time to gain a new equilibrium or not. However, since it is not clear from the physical point of view what the viscosity after an encounter is going to be, we need to just rely on the value that comes out of the SPH algorithm.

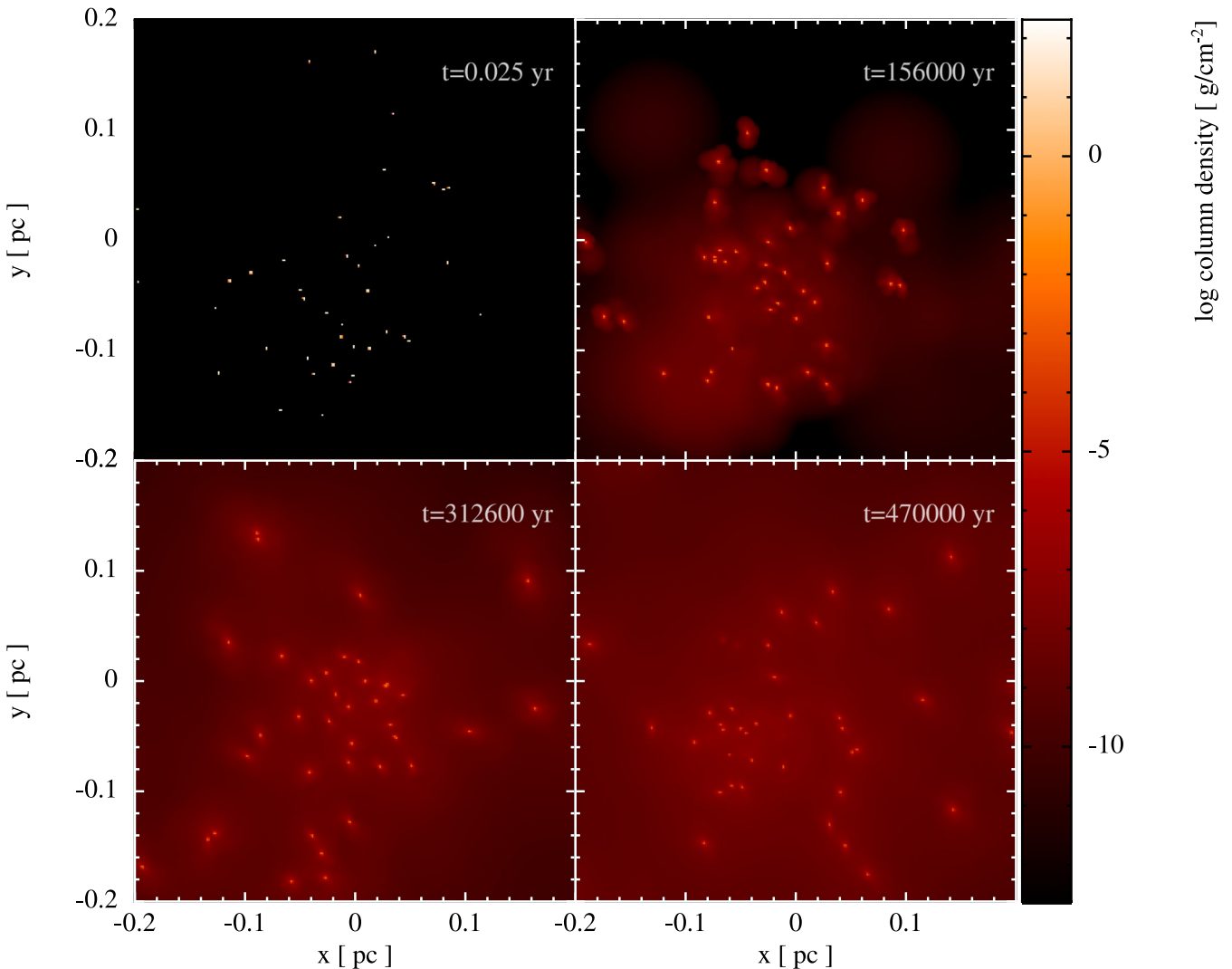
### 3.3 Simulation R10

We first comment in depth on the results from simulation R10, and use this as a reference to compare to the other simulations. Fig. 1 shows four column density snapshots from simulation R10. While at the beginning of the simulation the discs are so small that they are barely visible on the scale of the cluster, they expand significantly due to viscous spreading. Due to this expansion, the discs become large enough to be influenced by encounters. The interactions between stars produce some unbound gas, which is visible as a non-zero background density. The amount of gas that

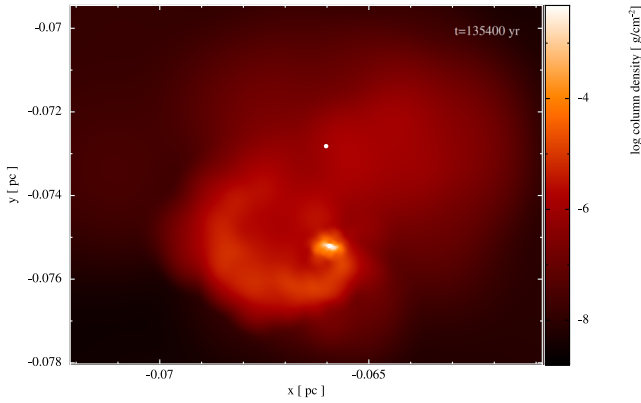
becomes unbound is small, and at the end of the simulation, the mass of the unbound gas is one order of magnitude less than the mass in all discs at  $t_{\text{end}}$ . Fig. 2 shows the detail of a disc during an interaction. The two stars are represented by the white dots (note that only one of them has a disc in this particular case). The tidal tail of gas that has been ejected from the disc (Toomre & Toomre 1972; Clarke & Pringle 1993) is clearly visible. We concentrate now on how the encounters affect the disc properties.

Fig. 3 shows the evolution of the discs in the cluster as a function of time for simulation R10. The left-hand panel shows the mass of the discs as a function of time, while the right-hand panel shows the radius of the discs as a function of time. The thick green line in the plot is a control run with a single star–disc system run in isolation. It is shown here as a reference, as it allows us to distinguish the effect due to the encounters. In isolation, the radius increases due to the redistribution of angular momentum due to viscosity and the mass decreases due to accretion on to the star.

The interactions between stars are stripping mass from the disc. The lines in the plot are coloured according to the distance of the closest encounter that each star had during the course of the simulation. The colour gradient shows that the closer the encounter,



**Figure 1.** Time evolution of the gas column density in run R10. The view is restricted to the central region of the cluster to help visualizing the gas distribution. Note that stars are not plotted.



**Figure 2.** Column density distribution at time  $t = 135\,400$  yr, showing the stripping of a disc shortly after the interaction of a star with a disc with a second star. The two stars are represented by the white dots. The tidal tail created during the interaction is clearly visible.

the stronger the effect in ejecting mass from the disc. In Fig. 4, we pick one of the discs that had a very close encounter (minimum distance smaller than 100 au), and plot against time both the disc mass (blue line) and the distance to the closest star at the given time (red dashed line). This clearly shows that the drops in mass are caused by close encounters.

In the right-hand panel of Fig. 3, the radius evolution is not completely smooth even for the disc in isolation. Here, the finite resolution certainly plays a more important role than for the mass, being an integrated quantity. Nevertheless, the effects of the encounters are much bigger than the noise for the disc in isolation. Some discs show big variations in the radius after an encounter, which is due to the fact that they are seeking a new equilibrium after they have been perturbed. It can be seen how nearly all the discs have smaller radii than the one run in isolation. To highlight this effect, we plotted also the median among all the discs, which shows the truncation effect of the encounters. The colour gradient is not so clearly visible here as in the left-hand panel. It can still be seen however that the discs that are significantly smaller than the disc in isolation experienced close encounters.

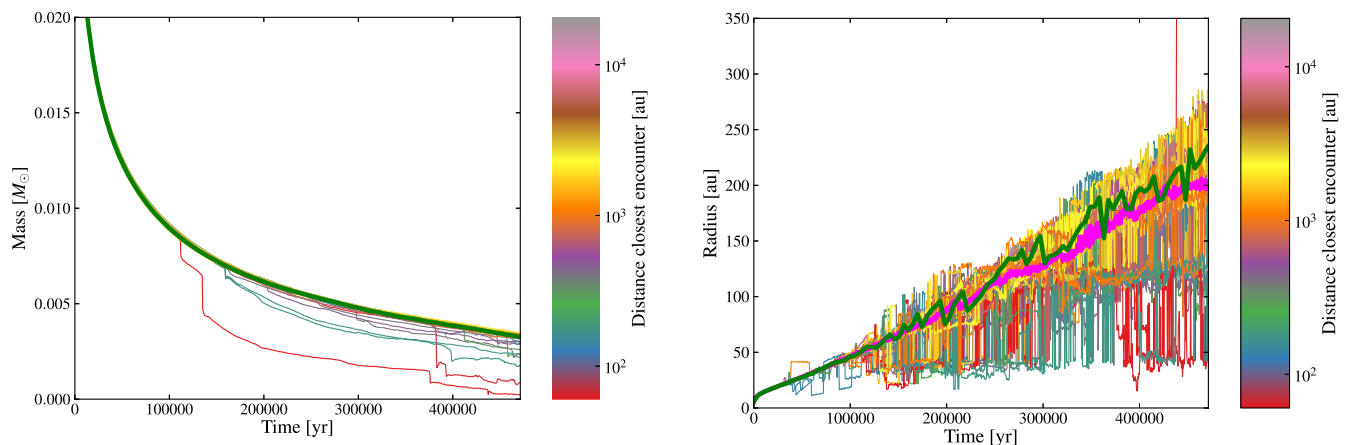


**Figure 3.** Left-hand panel: disc masses as a function of time. Right-hand panel: disc radii as a function of time. In both panels, lines are coloured by the distance of closest encounter that the star experienced, and the colour gradient shows how the closer the encounter, the more destructive the effect. The thick green line is the disc run in isolation. The thick magenta line in the right-hand panel is the median among all the discs, and shows the truncation effect of the encounters.

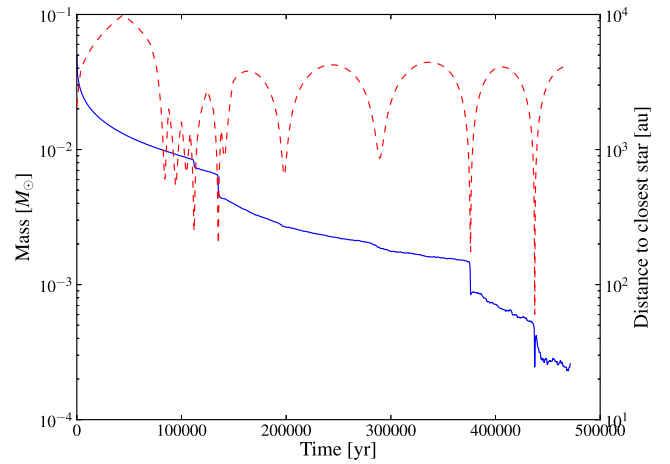


**Figure 4.** Mass versus time (blue solid line) and distance to closest star (red dashed line) for one disc from simulation R10. Sudden drops in mass are clearly caused by close encounters.

To further explore the dependence of disc parameters at  $t_{\text{end}}$  on the distance of closest encounter, we show in Fig. 5 the final disc radii and masses as a function of the distances of the closest encounter. Since the disc size varies in time, we normalize the distance of the encounter to the disc size at the moment of the encounter. The correlation in mass (left-hand panel) is quite strong, and confirms that the distance of the closest encounter is a good quantity to derive the mass lost in an encounter, even when disc spreading and mass accretion on to the central star are taken into account. This confirms qualitatively the validity of previous studies (e.g. Scally & Clarke 2001; Olczak et al. 2006) that used this parameter, either recording the single closest encounter, either the history of the most destructive ones, to quantify the importance of encounters in mass removal from the disc. However, due to the presence of accretion and spreading in our work, a detailed comparison with previous work is not possible. Note that, since the discs all start from the same initial conditions and follow the same evolution in absence of external perturbations, discs that experienced only distant encounters end up with the same value for the mass. We do not expect a real disc population to exhibit

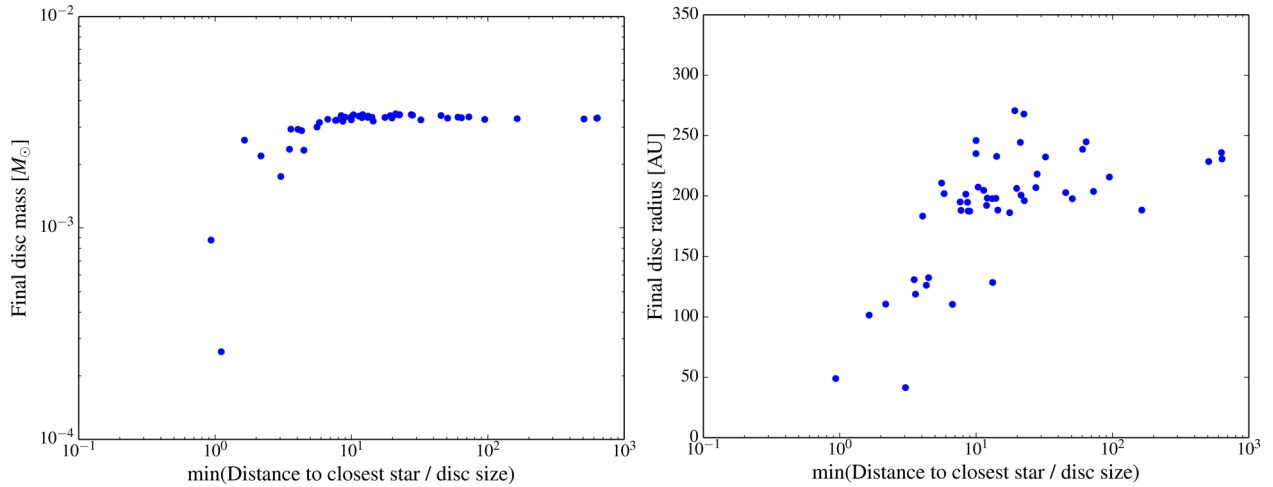


**Figure 5.** Left-hand panel: final disc mass as a function of the distance of closest encounter, in units of the disc size at the moment of the encounter. Right-hand panel: final disc radius as a function of the distance of closest encounter, in units of the disc size at the moment of the encounter. The correlation in the disc mass is quite remarkable, and shows how the distance of the encounter is a good quantity to use to derive the mass lost in the encounter. The correlation in the disc radius has more scatter (see the text for an explanation), which shows the importance of numerical simulations to quantify the influence of encounters on the disc sizes.

such behaviour, due to a spread in the initial conditions and in the evolution.

The right-hand panel shows that also the disc size at  $t_{\text{end}}$  correlates with the distance of the closest encounter. This shows the destructive effect of encounters, which are able to truncate the discs. It is instructive to compare this correlation with the mass one. The disc size is more sensitive to distant encounters than the disc mass (Fig. 5). In particular, distant encounters (e.g. 10–20 disc radii) do not affect the disc mass, but are able to modify the disc radius. Since a star also experiences other encounters than the closest one, they can also contribute to determine the final disc size. This is one of the reasons why the radius correlation has more scatter than the mass one.

In addition, after an encounter the disc spreads again, so that, given two discs that experienced a close encounter at the same distance but at different times, we do not expect the final sizes to be the same. This also means that, while we commented before that our simulations confirm the validity of semi-analytical approximations for inferring the disc mass, the same cannot be said for the disc

sizes. Numerical simulations are of primary importance here to get accurate determinations of the importance of dynamical interactions in shaping the disc size.

We show in Fig. 6 histograms for the final disc masses and radii. The red solid vertical line in both plots shows the value for the disc run in isolation, while the green dashed vertical line shows the median of the distribution. Few discs had close encounters that modified their masses significantly (Fig. 6, left-hand panel), as shown in Fig. 5, so that the median of the distribution is only marginally smaller than the value for the disc run in isolation. Therefore, although a close encounter can have a strong effect on the specific disc, close encounters are not frequent enough to significantly alter the disc masses on average. This is highly dependent on the initial conditions for the cluster, and the absence of high-mass stars certainly plays an important role, since it removes the source of the most destructive encounters. This will be discussed in a subsequent paper.

The effect of encounters on the distribution of final disc radii (Fig. 6, right-hand panel) is more evident, as most of the discs

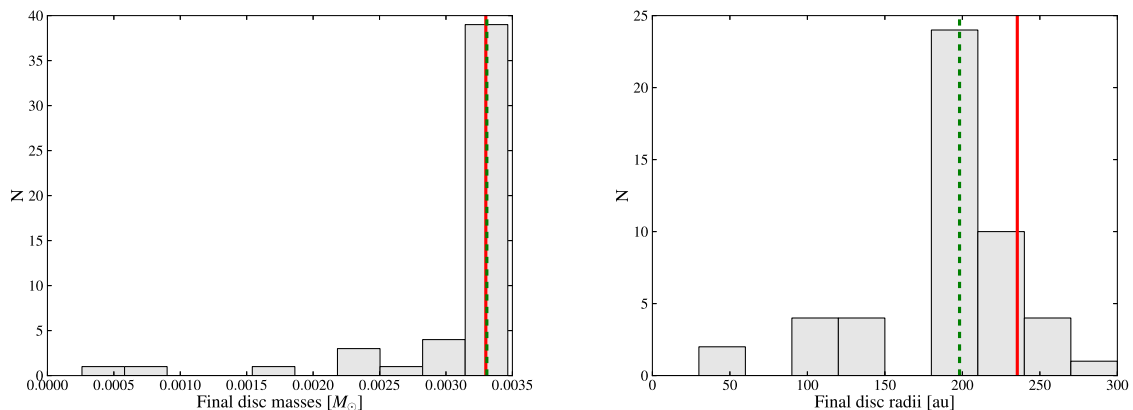


**Figure 6.** Left-hand panel: histogram of the final disc masses. Right-hand panel: histogram of the final disc radii. The red solid vertical line in both plots shows the value for the disc run in isolation, while the green dashed vertical line shows the median of the distribution. Although a close encounter can have a dramatic effect on the mass of the disc, few discs had such close encounters, so that the median of the mass distribution is not significantly affected. However, even distant encounters can change the disc radius, so that we see a change in the median disc radius when comparing with the disc run in isolation.

experience a reduction in size due to the encounters. A number of discs are truncated at very small radii. We will show in Section 4 that their final radii are compatible with having been truncated by the close encounters. There is also a number of discs which are not dramatically truncated, yet which are affected by more distant encounters. With respect to the disc in isolation, the final radius of these discs is reduced by  $\sim 10$ – $20$  per cent.

### 3.4 Simulations with larger initial radius

Fig. 7 shows the evolution of the radius for runs R30, R100 and R300. For simplicity, we show only the evolution of the median radius, compared with the disc in isolation. To compute the median, we excluded discs that experienced a significant mass loss (more than 99.5 per cent). As they are now only represented by a handful of SPH particles, the definition of radius ceases to be meaningful for them. Note that, for different disc sizes, the viscous time and the exponent in the expansion law change (see Section 3.2). It is clear that for run R300 we have entered a regime where the disc size is set by the encounters rather than from the size of the disc itself or from viscous spreading: the median no longer increases after  $\sim 2 \times 10^5$  yr. A similar behaviour, although only towards the end of the simulation, can be seen for run R100. The spreading of these discs happens slower, while the encounter importance increases due to the smaller ratio between the encounter distance and the disc size. This behaviour is not linear, however, as can be seen from the R30 and R100 runs: the radius of discs in run R30 is almost unaffected by encounters, while the effect on run R100 is visible, but smaller than in run R10. As discussed in Section 3.2, the discs in the different runs have different spreading rates. This brings the discs in run R10 to become almost as big as the discs in run R300 within the time-scale of the simulation, while the discs in run R30 and R100 are eventually overtaken by the ones in R10. This effect comes from the different viscosities that we have in the different runs, which in the SPH method we cannot control. However, it is an effect that we can calibrate for, and which shows the interplay between disc truncation and spreading.

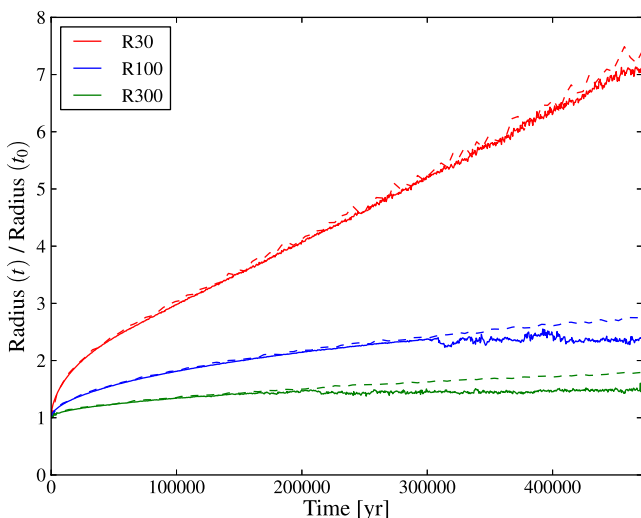


**Figure 7.** Evolution of the median disc radius for runs R30, R100 and R300 (see legend), in units of the initial disc size. The dashed line is the disc in isolation, while the solid line is the median of all the discs in the simulation. The median disc radius in run R300 no longer increases after  $\sim 2 \times 10^5$  yr, showing that we have reached a regime where encounters are limiting the disc size.

The mass histograms (left-hand panel of Fig. 8) shows that the runs with bigger discs had a handful of very destructive encounters, which produced discs with very small masses compared with the unaffected ones (note that in run R10, only a couple of discs had their mass reduced by an order of magnitude compared to eight discs in R300). This is expected, since for bigger discs the ratio between the distance of the encounter and the disc size decreases and the encounters become more penetrating. At the same time, however, the dependence of the final disc mass on the distance of the closest encounter (left-hand panels of Fig. 9), measured in units of the disc size, changes. While for run R10 the dependence is quite shallow, it is much steeper, almost a step function, for the other three runs. Stated in another way, the bigger discs are also more resistant to encounters, as only very close encounters are able to affect them. Therefore, while the close encounters produced a lot of damage in the discs, overall the encounters were not able to modify significantly the mass of the discs, because only a few of them were able to probe the left part of this step function. This can be seen also comparing the difference between the median mass and the disc in isolation, which is very small for all the runs. In short, the masses of small discs are not significantly affected, because the encounters are not penetrating enough; big discs are also not significantly affected, because they are more resistant to encounters.

One possible explanation for this different behaviour is that distant encounters cause a mass redistribution in the disc, ‘hardening’ the surface density (see Hall 1997). While this is washed out easily in run R10 by the higher viscosity, through disc spreading, this effect is not strong enough in the other runs. This accounts for the steeper relation observed in the correlation between the final mass and the distance of the closest encounter, as a small difference in the encounter distance can make a big difference in the mass involved in the encounter if the surface density is steep. We discuss this idea further in Section 4.1.

Another quantity of interest is the mass accreted on to the star. We show in Fig. 10 the accreted mass as a function of time for the discs in the simulation, with the four panels corresponding to the four simulations. While for the small discs there is little to no effect on the accreted mass, the encounters produce strong bursts in accretion for the bigger discs. Such bursts were already found in simulations by Pfalzner et al. (2008), and they have been proposed as an explanation for FU Orionis objects. However, we caution that numerical effects may also partially contribute to this result, since bigger discs also have bigger accretion radii. Therefore, while the result is interesting, further work is needed to assess its physical relevance. Interestingly, we note also that some stars that did not possess a disc at the beginning of the simulation may accrete some mass, which they have stripped in an encounter from a disc around another star. This could open the exciting possibility of reactivating accretion on a star that is already in the class III phase (i.e. has already dissipated its disc). Unfortunately it is difficult to quantify precisely how long such a burst would last and which accretion rates it could reach, due to the limited resolution available in terms of mass. We leave also this study for future work.

## 4 DISCUSSION

### 4.1 Understanding disc sizes

We show in Fig. 11 the results of the model presented in Section 2.3, compared with those from the simulation. For comparison, here we plot also the discs that experienced very close encounters. It can be noticed that sometimes the sizes derived from the simulation are

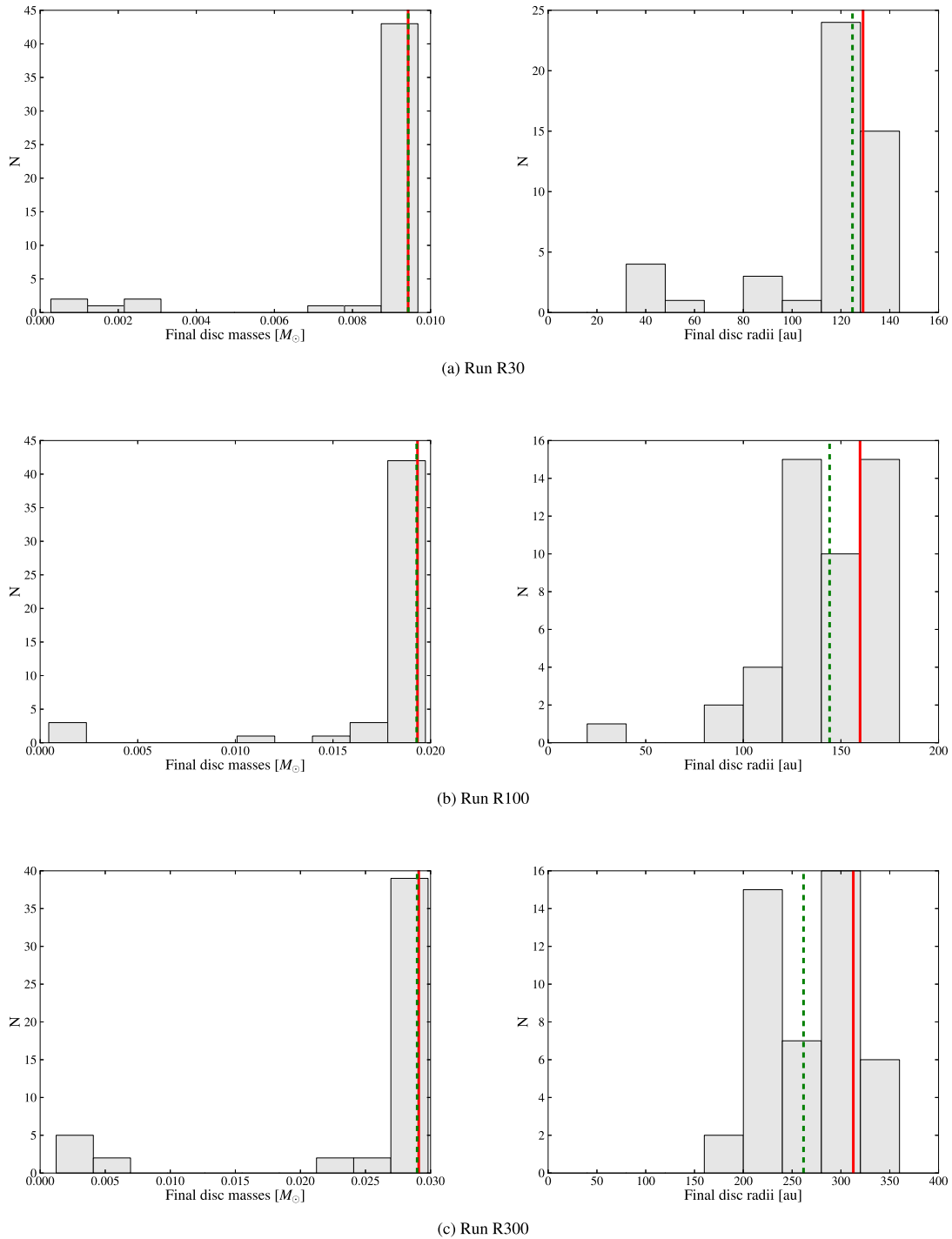


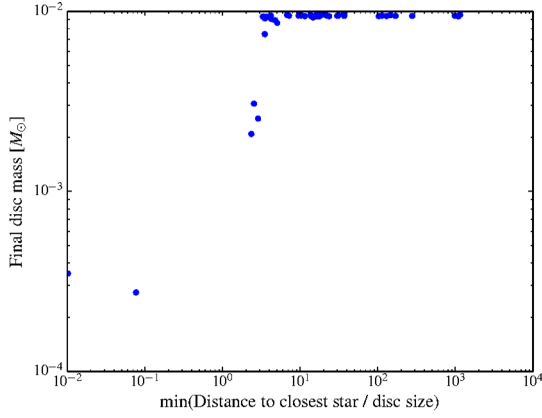
**Figure 8.** Left-hand panels: histogram of the final disc masses. The solid red line is the value for the disc in isolation, while the green dashed line is the median of the distribution. Right-hand panels: histogram of the final disc radii. The solid red line and the green dashed line have the same meanings as in the radii plot.

much bigger than the disc in isolation; this is because the very close encounter destroyed the disc, and therefore the notion of disc radius is no longer meaningful.

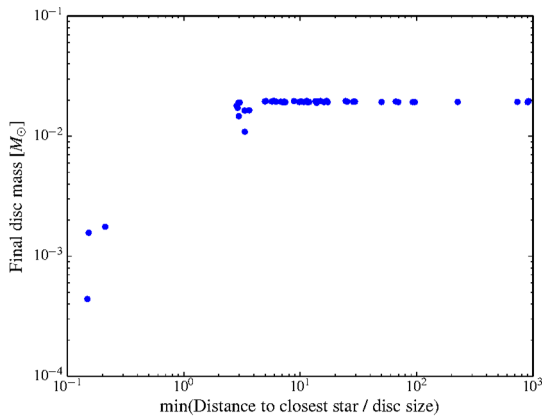
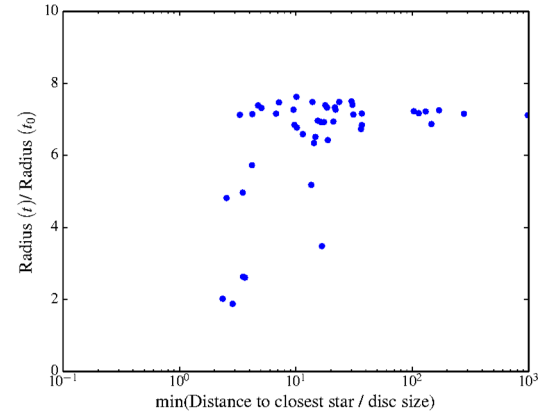
We note the very good agreement for run R10, which is remarkable for such a simple model. While it does not correctly predict the sizes of all the discs, it is still quite effective for most of them, and it correctly reproduces the correlation between the two quantities. While the agreement is not as good for the other runs, the model

still correctly identifies which discs have been severely affected by the encounters and which ones are not. In particular, by combining information from these plots and the ones shown previously, we can observe the following three different regimes.

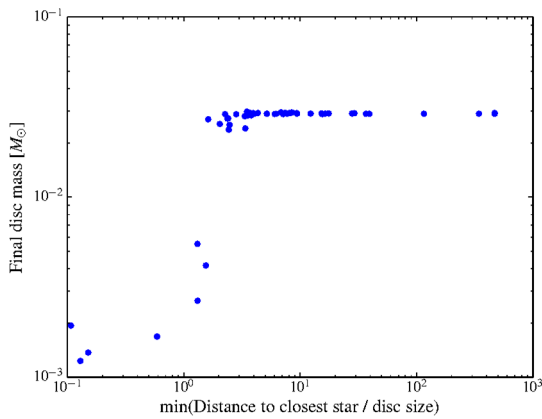
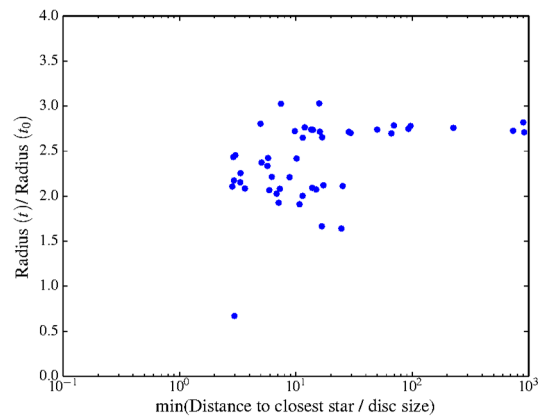
(i) Discs that had very penetrating encounters were significantly affected in their sizes. The assumption that discs are truncated at  $d/3$  made in the model correctly captures which discs are in this



(a) Run R30



(b) Run R100



(c) Run R300

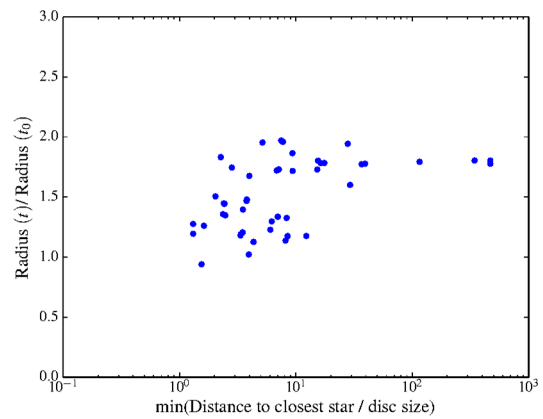


**Figure 9.** Left-hand panels: final disc masses as a function of the distance of the closest encounter, measured in units of the disc size at that moment. Right-hand panels: final disc radii in units of the initial size as a function of the minimum value of the ratio of the encounter distance to the instantaneous disc size.

regime, in line with previous findings (Clarke & Pringle 1993). Note that in run R10 discs sizes are sometimes reproduced even in this regime, while the model clearly fails for the other runs. To interpret this result, we note that discs in run R10 are undergoing much faster spreading, and so they are in a ‘spreading-dominated regime’. Viscosity is for them the main driver of evolution, and encounters act simply to truncate the disc. In the other runs, instead, a more complicated interplay emerges.

(ii) Discs that had only distant encounters, but which nevertheless are smaller than the disc run in isolation. This population is present especially in runs R100 and R300. This is a feature that the simple model does not catch. We suggest that this is due to the cumulative effect of many distant encounters, which modify the mass distribution of the discs, ‘hardening’ them (Hall 1997) and violating the assumptions of our semi-analytical model. In run R30, the discs did not grow enough to be significantly influenced by this effect; in

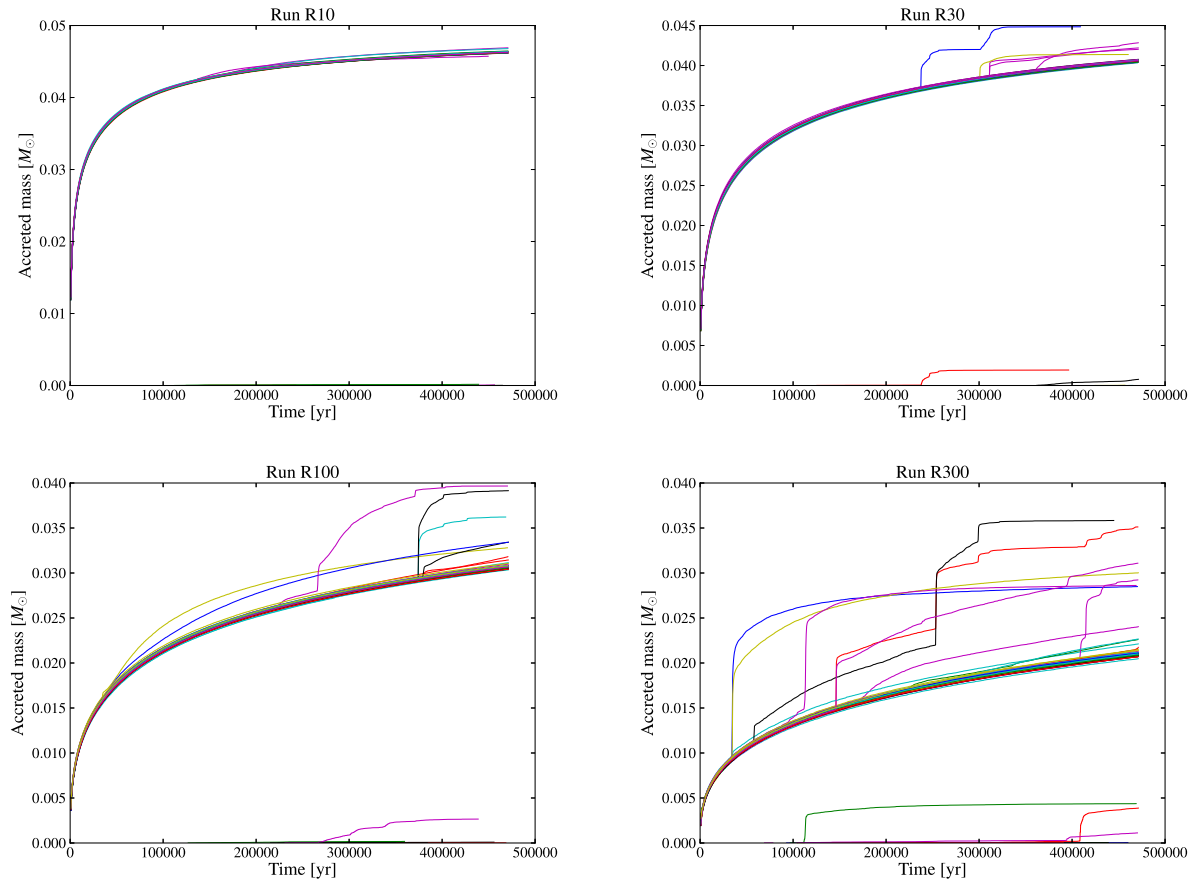


**Figure 10.** Accreted mass on the central star as a function of time for the four simulations run. Each line has a different colour to help distinguish them.

run R10, as previously mentioned the spreading is much faster, so that the steepening is being washed out by viscous evolution. Still, although this effect is smaller than in runs R100 and R300, also in run R10 there are discs that are a bit smaller than the prediction of the model, while still having had only distant encounters.

(iii) Discs that were largely unaffected by the encounters. The critical closest encounter to access this regime is of the order of 50 disc radii, but note that it is different in the different runs. In particular, the number seems to decrease with the initial disc size, which would point again in the direction of the big discs been ‘hardened’.

To check the hypothesis of modifications in the surface density distribution by the encounters, we fit the surface density at the end of the simulation with a power law (equation 4). We report in Table 2 the results. We list the values for the disc in isolation and for the median of the discs in the hybrid simulation. In the latter case, we fit only the discs that in the course of the simulation went above the threshold value of  $10^{-2} M_{\odot}$ , to avoid artefacts. As expected, simulation R10 shows very little difference between the isolation run and the median value, as it is the case for run R30. The steepening is instead clear in simulation R300, where the value of the median is well above the value of the disc in isolation. A hint of steepening may already be seen for run R100, with some caveats however: the surface density of the discs in this run tends to be quite steep even in isolation, another feature that is due to the behaviour of SPH viscosity at these low resolutions. Therefore, while the analysis shows that some hardening is taking place in simulation R300, we caution that the low resolution does

not allow us to measure quantitatively this effect. Future work will allow hardening to be studied more in detail. We note also that, if this effect is confirmed to be as big as measured here, it could be observationally probed by resolved observations of protoplanetary discs (Williams & Cieza 2011), which would allow one to verify if discs in dense environments have steeper surface density profiles than ones in sparse environments.

## 4.2 Comparison with observations

de Juan Ovelar et al. (2012) pointed out that observational data suggests a reduced disc size in environments with high stellar surface densities ( $\Sigma_{*}$ ). In particular, they looked at the measured disc size as a function of  $\Sigma_{*}$ . The population they consider is composed of 67 Class II objects in nearby SFR with radii measured through resolved imaging. The stellar density is computed with the Casertano & Hut (1985) method. Namely, one finds the  $N$  closest stars, defines  $d_N$  as the (projected) distance of the  $N$ th nearest neighbour and computes the surface density as  $(N-1)/\pi d_N^2$ . The data show a cut-off in disc sizes at stellar surface densities higher than  $\Sigma_{*} > 10^{3.5} \text{ pc}^{-2}$ . To highlight this cut-off, they perform a statistical test. They bin the data from higher to lower densities and for each bin they test with the Kolmogorov–Smirnov (KS) method if the distribution of the points in the bin is compatible with the distribution at lower surface densities.

We showed in the previous sections that the disc size is correlated with the closest encounter. In turn, the distance of the closest encounter depends on the environmental stellar density, but it is also a stochastic process; after experiencing a close encounter, the star

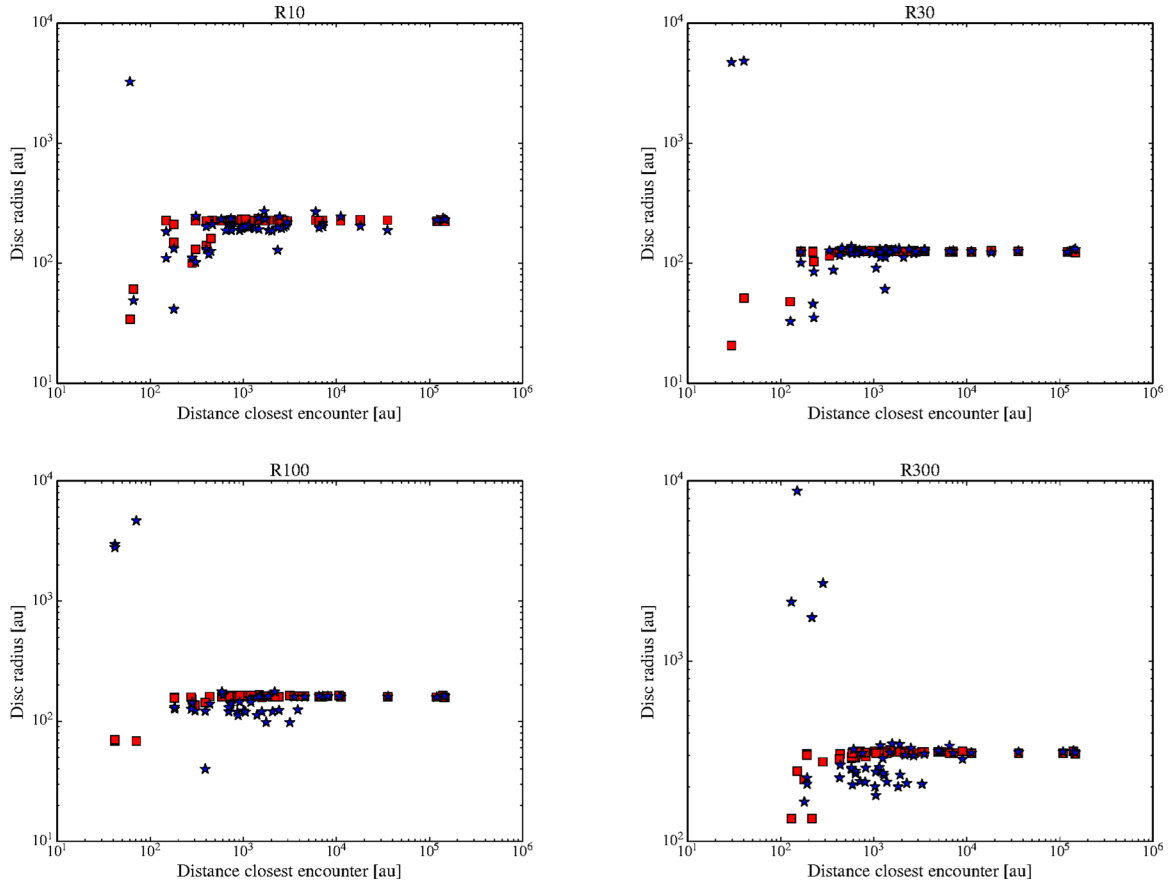


**Figure 11.** Comparison between the predicted disc sizes by the model (red squares) and the results from the simulation (blue stars). The different simulations are shown in order, from left to right and from top to bottom.

**Table 2.** We report for each run the power-law index  $p$  (equation 4) when fitting the surface density distribution. We list the values for the disc in isolation and for the median of the indexes obtained when fitting the discs in the hybrid simulation. The effect of steepening is evident in run R300 that has a higher value of the median with respect to the disc in isolation.

Run	$p$ isolation	$p$ hybrid
R10	0.56	0.55
R30	0.85	0.87
R100	2.34	2.47
R300	1.09	2.27

might move to a lower density region inside the cluster. Therefore, numerical simulations are of primary importance to assess what kind of correlation we expect theoretically in this parameter space, which can be probed by observations. It is important to have such predictions to distinguish from other candidates for the truncation of discs in clustered environments, such as external photoevaporation by massive stars.

First of all, we want to inquire how important is the movement of the stars in the cluster. The expectation to find smaller discs at high stellar densities relies on the fact that we expect the distance of encounters to depend on the local stellar density. However, this dependence could be washed out if a star experience a close encounter in a high-density region and then moves to a region with lower density. It is then important to check how important is this

effect. We follow Scally & Clarke (2001, see their appendix A) to build a semi-analytical model of the  $N$ -body dynamics in the cluster. We make the assumption that the stars keep their distance from the cluster centre of mass fixed, and so they experience a constant stellar density throughout the simulation. We then compute with a Monte Carlo experiment the distribution of the minimum encounter distance, and we compare it against the results of the simulation. We show in Fig. 12 the results. We plot the distance of the closest encounter (the blue dots are the results of the simulation) versus the distance from the centre of mass of the cluster. The red solid line is the median of the distribution drawn from the Monte Carlo experiment, which agrees with the results of the simulation. Therefore, it is indeed a good assumption to assume that the stars do not move systematically in the cluster over the simulation time-scale. This means that we expect the disc sizes to retain some information about the local stellar density. In addition, while we focused here mostly on the closest encounter, we note that a higher stellar density also enhances the number of encounters closer than a given distance, which also contributes to strengthen the correlation.

To check if dynamical encounters in our simulations can produce a feature like the one observed in the de Juan Ovelar et al. (2012) study, we go through the same exercise they carry out. We chose  $N = 20$  to compute the stellar surface density. Since our data are three dimensional, we show the results of projecting along three different axes (we chose the coordinate axes for simplicity). However, our simulations are carried out for different values of initial disc radius separately. Our radii versus ambient stellar density

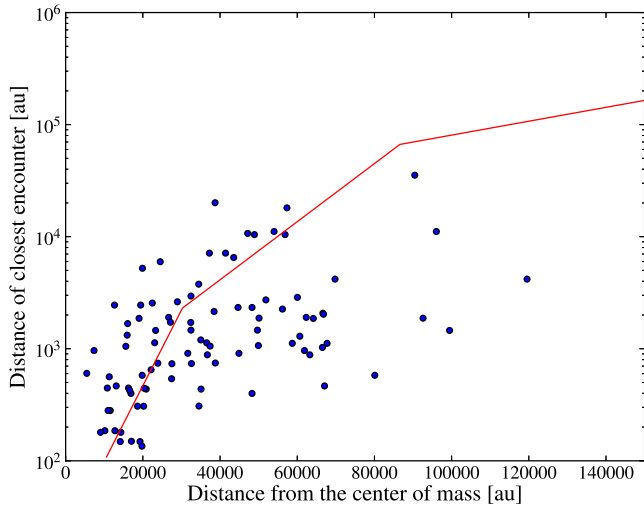


**Figure 12.** Distance of the closest encounter versus the distance from the centre of mass for each star. The dots are the results of the simulation, while the solid line is the result of the Monte Carlo experiment described in the text, which yields a prediction for the median of the distance of the closest encounter at each location.

distribution is strongly influenced by this initial condition. To generate a more realistic population, and therefore more similar to that of the de Juan Ovelar et al. (2012) study, we combine the discs in all four simulations into a single population conserving the separated projections on to the  $x$ -,  $y$ - and  $z$ -axes. We then perform the KS-test over this composite distribution for each axis separately. Fig. 13 shows the radii versus ambient surface stellar density distribution and the results of the test for each axis in the same format as in fig. 1 of de Juan Ovelar et al. (2012). To show the effect of the

bin size, we compute the KS-test for [20, 25, 30] elements per bin and our composite population has 192 discs. To avoid edge effects, we perform the test only over bins where the population at lower densities is larger than a sixth of the complete population.

The result is that, despite the fact that stars move in the cluster, there is still statistical evidence of a reduction in disc sizes at high stellar densities, namely above  $\sim 2-3 \times 10^3$  stars  $\text{pc}^{-2}$ . In particular, the data in the last bins systematically show a low probability of being compatible with the rest of the distribution. Note that these simulations did not explore the high stellar densities that are present in some of the real clusters (compare with fig. 1 of de Juan Ovelar et al. 2012), which can go up to the  $10^4$  stars  $\text{pc}^{-2}$  in the ONC, and we are thus just beginning to sample the cut-off. It is however very promising that the density at which this cut-off happens is consistent with the one found by de Juan Ovelar et al. (2012). We leave future work to assess this regime, where the inclusion of massive stars is also important. Future work will also explore higher resolutions than what is currently possible, and measure with more accuracy the exact threshold at which the cut-off takes place.

We also note that in the literature there are indications of other influences of the environment on protoplanetary discs. For example, Sicilia-Aguilar et al. (2011, 2013) consider the Coronet cluster, which having  $\sim 50$  stars inside 0.15 pc is not very dissimilar from our simulations. These authors find that discs in the Coronet cluster are more evolved than in the Tr 37 cluster. This is quite surprising, given that the Coronet cluster is 1–2 Myr old, while Tr 37 has an estimated age of 4 Myr. Their interpretation is that the difference is due to the much higher stellar density in the Coronet cluster. While our simulations do not yet allow for a detailed comparison with their results, this is an interesting path to be explored in future works.

Finally, in this work we have ignored the effect of external photoevaporation, with the goal to isolate the effect of the encounters. External photoevaporation is also a process that limits the disc size.

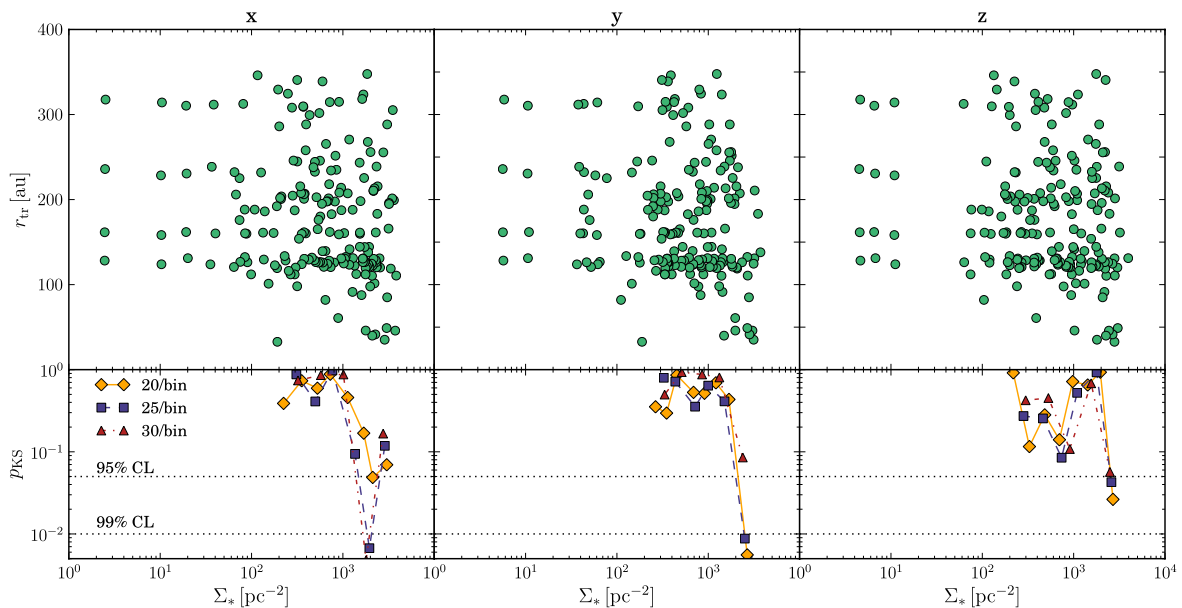


**Figure 13.** Projections along the three coordinate axes of the radii versus environmental surface stellar density ( $\Sigma$ ) distribution of the population of discs resulting from the combination of all discs in each of our four runs. The lower panels show the results of a Kolmogorov–Smirnov test where we bin the data and compare the distribution in each bin with the one of the discs at a lower stellar densities. The different symbols are for different number of elements in each bin. Although the stars move in the cluster, they still retain information about their original position, so that there is statistical evidence of a cut in disc sizes at high stellar densities. In particular, the probability of the last bin to be compatible with the rest is always low. Note however that this simulation did not explore the high stellar densities that are present in some of the real clusters (compare with fig. 1 of de Juan Ovelar et al. 2012).

Using a time-scale argument, Adams et al. (2004) estimated that a protoplanetary disc around a solar mass star would have its size reduced by external photoevaporation down to 30–60 au (depending on the assumptions on the disc viscosity) in a time-scale of several Myr. Clarke (2007) confirmed these results through the modelling of the viscous evolution of a protoplanetary disc undergoing external photoevaporation, and found a significant shrinking of discs around solar-mass stars down to  $\sim 100$  au after approximately 1 Myr.

These radii are much smaller than the final radii of the discs in our simulation. However, we remark that these authors simulate conditions ( $G_0 = 3000$ , where  $G_0$  is the value of the far ultraviolet field in the interstellar medium) which are more relevant for a massive cluster such as the ONC than for the cluster we simulate here. Indeed, the ONC is a spectacular example of the potential impact of external photoevaporation on protoplanetary discs. However, a cluster with only 100 stars is unlikely to have massive stars due to the limited sampling of the initial mass function, and therefore we do not expect any significant external photoevaporation to happen in it.

More massive clusters have instead a higher probability of hosting massive stars, increasing the importance of external photoevaporation. In addition, the importance of both external photoevaporation and encounters depend on the number density of stars, so that it is not trivial to understand which process would dominate. The picture is complicated even more by mass segregation that acts on different time-scales, making massive stars sink to the central dense regions more rapidly in low mass clusters. Nevertheless, if it is confirmed that external photoevaporation is more important than encounters in limiting disc sizes in massive clusters, then there must exist a threshold mass of the cluster where one switches from an encounter dominated regime to an external photoevaporation dominated regime. Further work is needed to include the effects of external photoevaporation in simulations like the one we conducted here and investigate these effects. While only a minority of all stars form in bound clusters (Lada & Lada 2003; Kruijssen 2012), up to 50 per cent of all stars forming in bound clusters do so in clusters of  $M < 10^3 M_\odot$ . Hence, both high- and low-mass clusters are worth exploring, which we plan to do in future work.

## 5 CONCLUSIONS

We have presented results from the first hybrid  $N$ -body–SPH simulations of coupled cluster and protoplanetary disc evolution. The discs in our simulation are expanding and accreting material on to the star due to viscous evolution, but they are also affected by close encounters between stars. Our simulations allow us to study whether a clustered environment, through the effect of encounters, modifies the protoplanetary disc evolution. We find that encounters can be very destructive for some of the discs, leading to almost complete dispersal for some of them. However, overall the median mass of the discs is not severely affected by the encounters.

We find that disc size is much more affected by encounters than disc mass. In the case in which disc spreading is fast, due to a high viscosity, only close encounters matter, as any mass redistribution in the disc caused by more distant encounters is quickly washed out. In this case, the close encounters simply truncate the disc at a given radius. If instead the spreading is not fast enough, we find a regime where distant encounters can have a significant impact on the discs, hardening their surface densities, and thus shrinking their radii. This also makes the discs more resistant to mass stripping by subsequent encounters. Therefore, we stress the importance of hydrodynamical

numerical simulations of this kind to yield accurate predictions of the impact of stellar encounters on disc sizes.

Finally, we confirm that theoretically we expect to see a cut-off at stellar densities higher than  $10^{3.5} \text{ pc}^{-2}$  in the disc sizes due to the effect of encounters. Further work is needed to probe the high stellar densities present in real stellar clusters.

## ACKNOWLEDGEMENTS

GR acknowledges the support of the International Max Planck Research School (IMPRS). This research was supported by the DFG cluster of excellence ‘Origin and Structure of the Universe’ (JED, DH, BE). We would like to acknowledge the Nordita programme on Photo-Evaporation in Astrophysical Systems (June 2013) where part of the work for this paper was carried out. We thank Cathie Clarke, Leonardo Testi, Carlo Manara, Antonella Natta, Henny Lamers and all the participants of the ESO Star Formation Coffee for stimulating discussions. We are grateful to the referee (Richard Alexander) for the constructive criticism. Our visualizations made use of the SPLASH software package (Price 2007). JMDK acknowledges the hospitality of the Aspen Center for Physics, which is supported by the National Science Foundation Grant no. PHY-1066293

## REFERENCES

- Aarseth S. J., Henon M., Wielen R., 1974, *A&A*, 37, 183  
 Adamo A., Östlin G., Zackrisson E., 2011, *MNRAS*, 417, 1904  
 Adams F. C., 2010, *ARA&A*, 48, 47  
 Adams F. C., Hollenbach D., Laughlin G., Gorti U., 2004, *ApJ*, 611, 360  
 Alexander R. D., Clarke C. J., Pringle J. E., 2006, *MNRAS*, 369, 229  
 Andrews S. M., Williams J. P., 2005, *ApJ*, 631, 1134  
 Armitage P. J., 2011, *ARA&A*, 49, 195  
 Artymowicz P., Lubow S. H., 1994, *ApJ*, 421, 651  
 Balsara D. S., 1995, *J. Comput. Phys.*, 121, 357  
 Bastian N., 2008, *MNRAS*, 390, 759  
 Bate M. R., Burkert A., 1997, *MNRAS*, 288, 1060  
 Bate M. R., Bonnell I. A., Price N. M., 1995, *MNRAS*, 277, 362  
 Casertano S., Hut P., 1985, *ApJ*, 298, 80  
 Clarke C. J., 2007, *MNRAS*, 376, 1350  
 Clarke C. J., Pringle J. E., 1993, *MNRAS*, 261, 190  
 Clarke C. J., Gendrin A., Sotomayor M., 2001, *MNRAS*, 328, 485  
 Craig J., Krumholz M. R., 2013, *ApJ*, 769, 150  
 Dale J. E., Ercolano B., Bonnell I. A., 2013, *MNRAS*, 430, 234  
 de Juan Ovelar M., Kruijssen J. M. D., Bressert E., Testi L., Bastian N., Cánovas H., 2012, *A&A*, 546, L1  
 Ercolano B., Clarke C. J., Hall A. C., 2011, *MNRAS*, 410, 671  
 Fedele D., van den Ancker M. E., Henning T., Jayawardhana R., Oliveira J. M., 2010, *A&A*, 510, A72  
 Forgan D., Rice K., 2009, *MNRAS*, 400, 2022  
 Goddard Q. E., Bastian N., Kennicutt R. C., 2010, *MNRAS*, 405, 857  
 Gorti U., Dullemond C. P., Hollenbach D., 2009, *ApJ*, 705, 1237  
 Guilloteau S., Dutrey A., Piétu V., Boehler Y., 2011, *A&A*, 529, A105  
 Gullbring E., Hartmann L., Briceno C., Calvet N., 1998, *ApJ*, 492, 323  
 Hall S. M., 1997, *MNRAS*, 287, 148  
 Hartmann L., Calvet N., Gullbring E., D’Alessio P., 1998, *ApJ*, 495, 385  
 Hayashi C., 1981, *Prog. Theor. Phys. Suppl.*, 70, 35  
 Heller C. H., 1995, *ApJ*, 455, 252  
 Herczeg G. J., Hillenbrand L. A., 2008, *ApJ*, 681, 594  
 Hubber D. A., Batty C. P., McLeod A., Whitworth A. P., 2011, *A&A*, 529, A27  
 Hubber D. A., Allison R. J., Smith R., Goodwin S. P., 2013a, *MNRAS*, 430, 1599  
 Hubber D. A., Falle S. A. E. G., Goodwin S. P., 2013b, *MNRAS*, 432, 711  
 Isella A., Carpenter J. M., Sargent A. I., 2009, *ApJ*, 701, 260  
 Johnstone D., Hollenbach D., Bally J., 1998, *ApJ*, 499, 758

Koepferl C. M., Ercolano B., Dale J., Teixeira P. S., Ratzka T., Spezzi L., 2013, *MNRAS*, 428, 3327

Kraus A. L., Ireland M. J., Hillenbrand L. A., Martinache F., 2012, *ApJ*, 745, 19

Kruijssen J. M. D., 2012, *MNRAS*, 426, 3008

Kruijssen J. M. D., Maschberger T., Moeckel N., Clarke C. J., Bastian N., Bonnell I. A., 2012, *MNRAS*, 419, 841

Lada C. J., Lada E. A., 2003, *ARA&A*, 41, 57

Lada C. J., Margulis M., Dearborn D., 1984, *ApJ*, 285, 141

Landau L. D., Lifshitz E. M., 2010, *Mechanics*. Elsevier Butterworth-Heinemann, Oxford

Lodato G., Price D. J., 2010, *MNRAS*, 405, 1212

Lodato G., Pringle J. E., 2007, *MNRAS*, 381, 1287

Lodato G., Meru F., Clarke C. J., Rice W. K. M., 2007, *MNRAS*, 374, 590

Longmore S. N. et al., 2014, in Beuther H., Klessen R., Dullemond C., Henning Th., eds, *Protostars and Planets VI*. Univ. Arizona Press, preprint (arXiv:1401.4175)

Luhman K. L., Allen P. R., Espaillat C., Hartmann L., Calvet N., 2010, *ApJS*, 186, 111

Lynden-Bell D., Pringle J. E., 1974, *MNRAS*, 168, 603

Malmberg D., de Angeli F., Davies M. B., Church R. P., Mackey D., Wilkinson M. I., 2007, *MNRAS*, 378, 1207

Malmberg D., Davies M. B., Heggie D. C., 2011, *MNRAS*, 411, 859

Manara C. F., Robberto M., Da Rio N., Lodato G., Hillenbrand L. A., Stassun K. G., Soderblom D. R., 2012, *ApJ*, 755, 154

Mann R. K., Williams J. P., 2010, *ApJ*, 725, 430

Miotello A., Robberto M., Potenza M. A. C., Ricci L., 2012, *ApJ*, 757, 78

Moeckel N., Bally J., 2007, *ApJ*, 656, 275

Monaghan J. J., 1997, *J. Comput. Phys.*, 136, 298

Monaghan J. J., Lattanzio J. C., 1985, *A&A*, 149, 135

Morris J. P., Monaghan J. J., 1997, *J. Comput. Phys.*, 136, 41

Murray J. R., 1996, *MNRAS*, 279, 402

Natta A., Testi L., Muzerolle J., Randich S., Comerón F., Persi P., 2004, *A&A*, 424, 603

O'dell C. R., 1998, *AJ*, 115, 263

Olczak C., Pfalzner S., Spurzem R., 2006, *ApJ*, 642, 1140

Olczak C., Kaczmarek T., Harfst S., Pfalzner S., Portegies Zwart S., 2012, *ApJ*, 756, 123

Owen J. E., Ercolano B., Clarke C. J., Alexander R. D., 2010, *MNRAS*, 401, 1415

Owen J. E., Ercolano B., Clarke C. J., 2011, *MNRAS*, 412, 13

Pelupessy F. I., Portegies Zwart S., 2012, *MNRAS*, 420, 1503

Pfalzner S., 2008, *A&A*, 492, 735

Pfalzner S., Vogel P., Scharwächter J., Olczak C., 2005a, *A&A*, 437, 967

Pfalzner S., Umbreit S., Henning T., 2005b, *ApJ*, 629, 526

Pfalzner S., Tackenberg J., Steinhausen M., 2008, *A&A*, 487, L45

Price D. J., 2007, *PASA*, 24, 159

Price D. J., Monaghan J. J., 2007, *MNRAS*, 374, 1347

Ricci L., Robberto M., Soderblom D. R., 2008, *AJ*, 136, 2136

Robberto M. et al., 2013, *ApJS*, 207, 10

Scally A., Clarke C., 2001, *MNRAS*, 325, 449

Shakura N. I., Sunyaev R. A., 1973, *A&A*, 24, 337

Sicilia-Aguilar A., Henning T., Kainulainen J., Roccatagliata V., 2011, *ApJ*, 736, 137

Sicilia-Aguilar A., Kim J. S., Sobolev A., Getman K., Henning T., Fang M., 2013, *A&A*, 559, A3

Silva-Villa E., Adamo A., Bastian N., 2013, *MNRAS*, 436, L69

Springel V., Hernquist L., 2002, *MNRAS*, 333, 649

Stolte A. et al., 2010, *ApJ*, 718, 810

Toomre A., Toomre J., 1972, *ApJ*, 178, 623

Walch S., Naab T., Whitworth A., Burkert A., Gritschneider M., 2010, *MNRAS*, 402, 2253

Williams J. P., Cieza L. A., 2011, *ARA&A*, 49, 67

**Table A1.** We report in the table the results of the resolution tests run.

Run	Resolution (particles)	$t_V$ (yr)	$\gamma$	$t_{\text{spread}}$ (yr)
R10	$10^4$	18 891	1.11	16 800
R10	$3 \times 10^4$	13 356	0.92	14 430
R10	$10^5$	20 584	1.02	20 080
R30	$10^4$	23 218	0.44	36 220
R30	$3 \times 10^4$	21 400	0.29	36 405
R30	$10^5$	14 600	-0.02	29 500
R30	$3 \times 10^5$	18 800	0.08	36 039
R100	$10^4$	11 760	-1.69	43 400
R100	$3 \times 10^4$	12 054	-1.84	43 600
R100	$10^5$	12 103	-1.93	47 640
R100	$3 \times 10^5$	19 763	-1.57	70 600
R300	$10^4$	25 430	-3.19	132 000
R300	$3 \times 10^4$	29 490	-3.17	152 750
R300	$10^5$	30 965	-3.26	162 950
R300	$3 \times 10^5$	35 710	-3.64	201 700

## APPENDIX A: RESOLUTION TESTS

In order to quantify the effect of the limited resolution available on viscosity, we run resolution tests of the discs in isolation. In addition to the runs presented in the text, which employed a resolution of  $10^4$  particles, we run simulations at resolutions of  $3 \times 10^4$ ,  $10^5$  and  $3 \times 10^5$  particles. For the smallest disc (run R10), we did not run the highest resolution case; being the smallest one, it is the one that requires the highest number of integration steps and therefore the strongest computational constraint. We then fitted the evolution of the radius of the disc as done in Section 3.2, obtaining the values reported in Table A1. It can be noted that increasing the resolution (in terms of number of particles) of a factor of 30 does not lead to a substantial difference in the spreading rates of the discs: the variation in  $t_{\text{spread}}$  is always less than a factor of 2. This change in the viscous time-scale can be explained by the change in resolution: as spatial resolution scales with  $N_{\text{part}}^{1/3}$ , the expected increase in spatial resolution is around 3.

This shows that, while it is certainly true that the spreading rates are enhanced by the limited resolution, the effect is rather small and is not likely to substantially affect our results and conclusions. In addition, the discs do not spread at a rate very incompatible with what is seen in observations. We note that higher viscosities cause the effect of encounters to be underestimated, since they would make viscous spreading more important. The good overall agreement of the semi-analytical model with the results of the simulations shows that, despite having rather large viscosities, the disc behaviour is still physical. The existence of a competition between disc spreading and encounters is therefore robust and has clear physical explanation.

This paper has been typeset from a  $\text{\TeX}/\text{\LaTeX}$  file prepared by the author.